Temporal Variations in a Four-Sheet Field-Aligned Current System and Associated Aurorae as Observed During a Polar-Ground Magnetic Conjunction in the Midmorning Sector

C. J. Farrugia

Institute for the Study of Earth, Oceans and Space, University of New Hampshire, Durham, NH

P. E. Sandholt

Physics Department, University of Oslo, Oslo, Norway

N. C. Maynard

Mission Research Corporation, One Tara Boulevard, Suite 302, Nashua, NH

R. B. Torbert

Institute for the Study of Earth, Oceans and Space, University of New Hampshire, Durham, NH

D. M. Ober

Mission Research Corporation, One Tara Boulevard, Suite302, Nashua, NH

Abstract

We relate measurements of temporarily varying field-aligned current systems (FACs) and their associated plasmas made by the Polar spacecraft at midmorning local times and likewise temporarily varying aurorae observed from Svalbard, Norway, when the magnetic footprint of the spacecraft passed across the field-of-view of the ground instruments on December 3, 1997. We combine the *in situ* observations of plasma, and magnetic and electric fields with meridian scanning photometry and all-sky imagery

from the ground site. The interplanetary magnetic field (IMF) pointed strongly east ($B_y >> 0$) and generally south. Descending from ~7.5 to ~5.5 R_E and heading south, Polar traversed a four-sheet current system: a twin-sheet cusp current system C1-C2, spanning 80.6°–77.7° invariant latitudes (ILT), and then the traditional regions 1 (R1) and 2 (R2) currents, extending from 77.7° to 73.3° ILT. A convection reversal separated the C1-C2 from the R1-R2 FACs. Currents C1 and R2 flow out of the ionosphere, while C2 and R1 flow into the ionosphere. Within C1, Polar observed six bursts of ions of typically magnetosheath energies ($\leq$ 2 keV) repeating every ~5 min, accompanied by intensified field-aligned electron beams and magnetic field depressions. Auroral data, acquired later but under very similar IMF conditions and at the same latitudes as when Polar was within C1, suggest auroral forms which are pulsed in both red and green lines with a similar period to the plasma bursts observed earlier at Polar. Within C2, at Polar, the pulsing ceased, but magnetosheath plasma was still present, albeit at diminished intensity. This was in part also a temporal change as the IMF clock angle decreased to ~60°. Equatorward of the cusp aurora we find a mixing region of magnetosheath and magnetospheric plasmas with spectral characteristics of the boundary plasma sheet (BPS) forming the source of the R1 current. Plasma inhomogeneities and bipolar current elements embedded therein were related to discrete east-west aligned arcs located equatorward of the cusp aurora. Within R2, when Polar was sampling the central plasma sheet, a field line resonance was observed on Polar and the underlying ground station HOP. A steady southward IMF rotation elicited a continued equatorward migration of all aurorae. Observations within C1-C2 are

discussed within the conceptual model of *Taguchi et al.* (1993), but extended to include the time dependent aspect so prominent in our observations. We thus hypothesize that the observations are due to time-varying reconnection under positive B_y conditions. The passage of the resulting reconnected flux tubes are registered at Polar as ion bursts whose lack of significant energy-latitude dispersion is likely due to the fact that Polar descends by only 1.1 degrees as it traverses the C1 current.

1. Introduction

Inside the magnetosphere large-scale field aligned currents (FACs) commmunicate electromagnetic stresses from high to low altitude regions (magnetospheric-ionospheric [M-I] coupling), keeping the ionosphere and magnetosphere moving together. Previous studies have shown that around local noon, besides the traditional regions 1 and 2 (R1 and R2) currents (*Armstrong and Zmuda*, 1973; *Iijima and Potemra*, 1976), another FAC pair poleward of these may also be present. The direction of current flow (into, or out of, the ionosphere) in these so-called cusp/cleft currents is found to be dependent on the sign of the IMF east-west component B_y (*Doyle et al.,* 1981, *Erlandson et al.*, 1988, *McDiarmid et al.*, 1978, *Ohtani et al.*, 1995). However, there is debate as to whether the cusp/cleft currents form large-scale currents independent of the R1 and R2 currents (i.e., with a different generating mechanism) or whether the lower latitude member of this pair is continuous with, and part of, the R1 current across noon (depending on the sign of B_y) (see *Erlandson et al.*, 1988; *Maynard et al.*, 1991; *Taguchi et al.*, 1993, and references therein). On the basis of an empirical model derived from DE-2 observations, *Taguchi et al.*, (1993) suggested that the source of the cleft-cusp currents is separate from R1/R2, even though the lower cusp-cleft current may be in the same direction as, and continuous with, R1. They proposed the electric field that is generated when magnetosheath plasma streams across the rotational discontinuity magnetopause onto field lines that have just reconnected at the dayside magnetopause as the source. From theoretical considerations, *Lee et al.* [1985] also derived a separate system of

cusp currents, originating at magnetopause rotational discontinuities, in the form of leakage along the magnetic field to the ionosphere of currents at the magnetopause. During B_y positive conditions, this cusp current consists of two components, one of which is directed into the ionosphere in the equatorward part of the cusp, and the other component is directed out of the ionosphere on the downstream, high-latitude side of the cusp.

In their models, *Taguchi et al.* (1993) and *Lee et al.* (1985) focussed on steady-state conditions. We present a case study of dayside FACs at midmorning local times (MLTs) which includes their time variability, an important feature of our observations. We use a complement of instruments at two altitudes. Data are shown from the magnetic, electric and plasma (electrons and ions) instruments on the Polar spacecraft in the altitude range ~5.5-7.5 R_e and meridian scanning photometers (MSP) and all-sky cameras (ASC) located at Ny-Ålesund, Svalbard (76° magnetic latitude [MLAT] or 75.8° invariant latitude [ILT]). The ground instruments view the polar cap boundary continuously during the winter observing season. The measurements were made during a magnetic conjunction between Polar and Svalbard which occurred on December 3, 1997. Interplanetary conditions are monitored at good resolution by the Wind spacecraft. Ancillary data include the records of the ground magnetometers from IMAGE/Svalbard (*Lühr*, 1994).

This is the second Polar-Svalbard conjunction in this pre-noon cusp - boundary layer region that we have studied. In a previous conjunction 3 days earlier (November 30, 1997; *Farrugia et al.* [2000]; *Ober et al.*, [2000]), the IMF was mainly northward-pointing

with brief southward excursions, and IMF $B_y < 0$. Inside the R1 current, Polar observed a region which was composed of particles of both high and low energies originating in the boundary plasma sheet (BPS), which we called there a "mixing region", borrowing the term from *Fujimoto et al.* [1998a], who described a similar spatial feature observed by Geotail. The mixing region was on sunward convecting magnetic field lines. The magnetospheric component was relatively enhanced in discrete plasma inhomogeneities. In the aurora, at the feet of these inhomogeneities, we observed multiple east-west aligned auroral forms, and we thus ascribed the plasma source of the R1 current on this pass to the mixing region, and the source of these auroral forms to these embedded inhomogeneities. Based on single-point measurements at Polar, these plasma inhomogeneites were termed "filaments" by *Farrugia et al.* [2000]. In view of their association with east-west aligned auroral forms, a term which reflects their geometry better is sheet-like plasma inhomogeneities. Below we shall use the generic terminology "plasma inhomogeneities".

In the R2 current, which was due to central plasma sheet (CPS) particles, we found magnetic oscillations and field line resonances (FLRs) in the Pc 5 frequency range. Correspondingly, the diffuse, green line aurora was pulsing at the same frequency. *Farrugia et al.* [2000] did not report on cusp currents.

In contrast, the pass on December 3, 1997, was dominated by IMF $B_y >> 0$ and was characterized by an IMF in which B_z on average pointed south with brief northward turnings. Thus this pass is complementary to that on November 30, 1997 and motivates our study of the control of M-I coupling at midmorning high latitudes by the IMF.

We shall first confirm the findings of the earlier work as regards the structure of the R1 and R2 currents and its relation to the aurorae, and unravel further structure in these FACs. A clear feature of the observations on December 3, 1997, is the presence of FAC cusp currents (called hereunder C1 and C2), with which we suggest an auroral response. At Polar, episodic bursts of an ion-electron plasma of magnetosheath energies and perturbations of the magnetic field are evident in the C1 current. While we have no auroral images during the time when Polar is crossing C1, in the auroral images acquired $\sim$1 hour later under very similar IMF conditions as during Polar's C1 traversal and in the same latitude range, we observe intensifications in the aurora repeating at a frequency similar to that of the plasma bursts at Polar.

Later in the event interval, all aurorae, both diffuse as well as discrete, drift significantly equatorward, and enhanced intensities are evident in both discrete arcs and cusp aurorae as the IMF B_z rotates further southward.

We shall interpret the observations of the cusp currents in terms of reconnection, following the conceptual scheme proposed by *Taguchi et al.* (1993). As noted, these authors addressed only the steady state aspects. We must also include variations in the reconnection rate.

A general note is in order about our interpretation. The observations by Polar of current structures, and when they occur, have both spatial and temporal aspects. The interplay between the spatial and the temporal is a subtle and involved issue, which is difficult to resolve with data from a single spacecraft, which is moving slowly across the structure. Boundaries move, and may do so more rapidly than the spacecraft movement.

Inflation of the magnetosphere in response to a pressure decrease is an obvious response. Since merging erodes the dayside magnetopause, there may also be an inflation of the magnetosphere when merging is slowed. In our opinion, there is a spatial 'substratum' in the current structure on top of which are superimposed changes in response to IMF variations. This temporal/spatial dichotomy has to be borne in mind when following the description of the observations and our interpretation thereof.

2. Conjunction Geometry

Figure 1 shows a geographic map centered around the ground optical site in Svalbard. Greenland is to the west (left) and mainland Scandinavia is to the south (down). We have drawn in the 76° MLAT (= 75.8° ILT) meridian passing through the ground site at Ny-Ålesund. The circle shows the approximate field-of-view of the ASC up to 70° zenith angle for the red auroral emission (630 nm), assuming an emission altitude of 250 km. The MSP scanning direction is indicated by the double-arrowed line. The symbol MN on this line designates magnetic north. The broad arrow at top right points toward noon. The magnetic footprint of Polar for the interval 0330 – 0730 UT is also shown in the same geographic coordinate system. It is mapped by the Tsyganenko (1989) model for a Kp value of 1, which was the value recorded during the event interval. The labels C1, C2, R1 and R2 on the footprint trace refer to the large-scale current systems traversed by Polar, as inferred from the local fields and plasmas discussed in section 4.1. We shall be concerned with the period 0412-0600 UT during which Polar's footprint lies within the field of view of the ASC, passing somewhat

Figure 1

to the east of the station. To help visualize the Polar-aurora correspondence, we have indicated the latitudinal zone of the cusp emission as observed by the MSP (at 630.0 nm) in Ny-Ålesund (between zenith angles 30 NZ-60 NZ) by two heavy, dashed lines. This is discussed in section 5.2.

3. Interplanetary Observations: Wind

Interplanetary plasma and magnetic field data from the Solar Wind Experiment (SWE; Ogilvie et al., 1995) and the Magnetic Field Investigation (MFI; Lepping et al., 1995) on the Wind spacecraft, respectively, are shown in Figure 2. The data are at ∼90 s (plasma) and ∼3 s (magnetic field) resolution. During the interval shown, Wind is at an average position of (199.4, 1.0, 26.5) R_E (GSE coordinates). Plotted from top to bottom are the proton density, bulk speed, temperature, dynamic pressure, total field and its GSM components, the IMF clock angle (i.e., polar angle in the GSM YZ plane), and the IMF cone angle (angle between the IMF and the X-direction). With an average convection speed of 350 km s^{-1}, and taking into account a slower transit through the magnetosheath, we estimate a delay for interplanetary parameters to affect the dayside magnetosphere/ionosphere of ∼70 min. The specific number quoted is obtained from a correspondence between IMF observations in the interval labeled I in the bottom panel and particle observations on Polar, discussed in section 4.3. The time axis in Figure 2 has been shifted forward by this amount. Generally, Wind observes a slow (< 400 km s^{-1}) solar wind of below-average dynamic pressure (~ 1.5 nPa) with an IMF oriented east and having a variable southerly component. Key times are indicated by vertical

Figure 2

guidelines. The conjunction interval (0412-0600 UT) is bracketed by the two outer guidelines. The first guideline marks the passage of a field directional discontinuity at which the IMF undergoes a sharp southward turn. A steady southward IMF rotation persists throughout this first interval. The second guideline marks the passage of an interplanetary field and flow discontinuity at which the IMF turns abruptly north. An ~18 min period of generally northward and eastward IMF follows (interval II). The rest of the conjunction interval is further subdivided into intervals III and IV. In intervals I-IV, the IMF is oriented south-east, north-east, east, and again south-east, respectively. Except for II, B_y lies in the range (3, 5) nT and generally $|B_y| \geq |B_z|$.

Interplanetary conditions in IMF interval I are very similar to those in interval IV: values of plasma parameters in the two intervals are nearly equal and the IMF components are of comparable strength and of the same polarity: $B_x < 0$, $B_y > 0$, and a slowly decreasing $B_z < 0$. Since no ASC images are available in interval I, we shall use this similarity to relate the aurora seen during interval IV to the Polar plasma observations made in interval I. It is thus stressed that the aurora-particle correspondence we shall suggest for interval I (labeled "cusp aurora" in Figure 1) is being inferred rather than being directly established with twin-altitude observations at the same time. Related to this we note that from 0515 - 0600 UT all data were available from both sites for the ground-Polar conjunction.

4. Polar Observations

In this section we discuss Polar observations made by three instruments: the magnetic field data from the MFE instrument (*Russell et al.*, 1995), which are at 6 s resolution; the particle data from the HYDRA instrument (*Scudder et al.*, 1995), shown at a resolution of 1.15 s; and the electric field data (EF; *Harvey et al.*, 1995) at 6 s resolution.

4.1. Magnetic field: Identification of large-scale current systems and their perturbations

Figure 3 displays the MFE measurements for the interval 0400 – 0600 UT. GSM coordinates are used and the IGRF-1995 reference field has been subtracted out. Quantity DB in the last panel is the total observed field strength less the total model field strength. The ILT of the spacecraft is shown at bottom. Using an infinite current sheet approximation, the changing gradient of the east-west component DB_y indicates the presence of 4 large-scale currents (two pairs of current sheets), labelled C1, C2, R1 and R2 in descending order of latitude. The R1-R2 boundary is chosen primarily from the changes in character of the electric field variations and the onset of plasma sheet electrons (shown below). The C2-R1 boundary is picked because of the change in character of DB_y, the convection reversal, and the change in character of the electrons. The C1-C2 boundary is chosen from changes in DB_y and the electrons. In C1 (0412 – 0447 UT) and R2 (0534 – 0600 UT) the eastward component (positive DB_y) is enhanced, which at midmorning northern latitudes indicates a current flowing out of the

Figure 3

ionosphere, denoted by "up" in the figure. Conversely, current flows into the ionosphere in sheets C2 (0447 – 0505 UT) and R1 (0505 – 0534 UT) ["down"]. The currents C2 and R1, which are spatially contiguous, have different levels of magnetic fluctuations. The invariant latitude extent of these currents are as follows: 80.6-78.8° (C1), 78.8-77.7° (C2), 77.7-75.1° (R1), and 75.1-73.3° (R2).

The above bracketing of the currents is basically a spatial interpretation of the variations and in a sense assumes that the driving conditions are constant over the interval. This is far from being the case, as can be seen from the IMF variations between the outer vertical lines in Figure 2. We note that with the suggested lag time in Figure 2, the current boundaries are close to times when the IMF changes. We will come back to the temporal aspects of the variations in the discussion. Because the boundaries are keyed by features in the Polar data, we will continue with their "spatial" definitions as we present the data.

Small-scale fluctuations of different character are superposed on all the large-scale currents in Figure 3. In C1 the total residual field exhibits 6 pulse-like depressions of ∼3-4 min duration, marked by vertical arrows in the bottom panel, which are accompanied by magnetic defections in the other components. The level of fluctuation is lowest in C2, and no impulsive field signatures are observed in this current. Using the suggested lag time, the average clock angle is 120° and 60° in C1 and C2, respectively [Figure 2]. In R1, large-amplitude, discrete perturbations in the components are visible which are mainly transverse to the background field, as can be seen from the relative amplitude of the fluctuations in the transverse components and the total field strength.

In R2, oscillations of period ∼7.5 min (frequency ∼2.2 mHz) are evident.

In summary, dividing the downward current by changes in its properties, we identify four large-scale currents flowing in two pairs of adjacent sheets. Consistent with previous work in this MLT sector for a positive IMF B_y (see, e.g., *Taguchi et al.*, 1993, and references therein), we identify the C1/C2 current pair as cleft currents; and the R1/R2 pair as the traditional region 1 and region 2 currents (*Iijima and Potemra*, 1976). Fine structure peculiar to each current system is evident. We shall use the current regimes shown in Figure 3 to organize the presentation and discussion of the rest of the observations.

4.2. Electric Field: Total potential drop and convection reversal

Figure 4 shows the electric field data. The top panel gives the electric potential along the spacecraft track in kV. The potential was found by integrating the along-track electric field, and the zero potential is arbitrarily set where the integration begins. The bottom panel shows the electric field along the spacecraft track in mV m^{-1}. From the latter, the sense of motion of the plasma may be inferred: the flow is antisunward when the electric field is negative, and sunward otherwise. The boundaries of the currents C1, C2, R1, and R2 from Figure 3 are also shown.

Figure 4

Across the large-scale current systems, the potential drop is modest (∼ 10 kV) and peaks at the convection reversal at ∼ 0505 UT, which coincides with the chosen C2/R1 interface. The largest potential difference is across current R1. Within C1 the flow is on average slowly antisunward (average electric field = -0.22 mV/m). Antisunward flow

picks up strongly in C2. Currents R1 and R2 are both on generally sunward flow. The fluctuations in both, which are of different character just as in the magnetic field, reflect the different structures in R1 (plasma inhomogeneities and current elements, see below) and R2 (quasi-periodic field fluctuations, see below). Noteworthy is the large bipolar electric field signal at 0515 UT. As we shall see, HYDRA saw an enhancement of low energy electrons at this time, and the bipolar electric field signal is also correlated with a discrete arc described below.

4.3. Polar/HYDRA observations: Pulsing plasma

Figures 5-7 present Polar/HYDRA observations. Figure 5 displays from top to bottom the ILT of the spacecraft, the differential energy fluxes (E_D) for protons and electrons, with intensities color-coded according to the respective scales on the right; and pitch angle-averaged energy and number fluxes (electrons in red) integrated over energy from 40 eV to the instrument threshold of 19.620 keV. Position information is given at the bottom. The label 'E'_D in the energy panels stands for "E Debye" to indicate that the differential energy fluxes have been shifted by the spacecraft potential. The current intervals C1, C2, R1, R2 defined in Figure 3 are denoted by vertical guidelines in the top panel. As shown in Figure 1, Polar is following a trajectory close to the 0900 MLT meridian and travelling southward at a radial distance which decreases from $R = 7.46$ R_E at 0400 UT to $R = 5.51$ R_E at 0600 UT. The ILT decreases from 81.1° to 73.3°.

Figures 5-7

Figure 5

After exiting the polar cap near 0410 UT, the spectral characteristics undergo significant changes during the interval shown. The spacecraft encounters a region

characterized by sporadically intensified electron and ion fluxes from ~0412 UT to ~0447 UT, i.e., within the C1 current. A pulsed sequence of ion bursts and electron intensifications are seen in the energy ranges of a few x 10^2 eV – ~1 keV, and < 300 eV, respectively, on top of a more tenuous population extending to higher energies in both components. The energies in the intense, pulsed plasma are magnetosheath-type values. The ion pulses are practically dispersionless. Six major pulses are observed between ~0420 – 0445 UT, corresponding to an average recurrence period of 5 min. The arrows in panel 4 mark the times when depressions in the magnetic field within the C1 current were observed by Polar/MFE. It is found that they all align well with the times when the ion pulses occur. The field depressions are thus seen to be a diamagnetic effect caused by these discrete plasma bursts.

At this point we discuss the IMF delay time we have been using (70 min). It was obtained as follows: the period of intense, pulsed magnetosheath plasma is made to coincide with IMF interval I, when the IMF has a continuous southward component. Its relatively abrupt termination then coincides with the abrupt northward turning of the IMF.

The electron behavior in C1 and C2 is shown in Figure 6. The panels display from top to bottom the differential energy fluxes antiparallel ($J_{-\|}$), perpendicular ($J_\perp$) and parallel ($J_\|$) to the magnetic field (pitch angle ranges 150°-180°; 75°-105°, and 0°-30°, respectively), the electron anisotropy (= $(J_{-\|} + J_\|)/2\ J_\perp$)) on a logarithmic scale, the omnidirectional energy flux and the number fluxes parallel and antiparallel to the magnetic field (parallel in red). During the ion events, the electrons form bidirectional

Figure 6

beams along the magnetic field with balanced parallel and antiparallel number fluxes.

A diminution in electron and ion fluxes and a transition to a more homogeneous population where pulsing is absent is observed between 0447 UT and 0505 UT (Figures 5 and 6). Average energies of ions and electrons are similar to those in C1. At this time Polar is within the downward current sheet C2 (Figure 3). A diminution in the magnetic fluctuation level with respect to C1 is also noted.

Between 0505 – 0534 UT, Polar traverses a plasma region characterized by a coexistence of the low and high energy electron and ion populations (a "mixing region", see *Farrugia et al.*, 2000). Sporadic, localized enhancements of the higher energy, magnetospheric component are present along with the magnetosheath-like components. (A clear example can be seen in Figure 5 near 0512 UT.) In relation to the magnetic field (Figure 3), these plasma inhomogeneities constitute a fine-scale structure embedded in the R1 current. The mixing region is flowing sunward (Figure 3). The structured electron and ion fluxes in the mixing region are typical of boundary plasma sheet (BPS) origin [see *Farrugia et al.*, 2000; *Ober et al.*, 2000].

The detailed view of the electron behavior during the period 0500 – 0540 UT is shown in Figure 7 in the same format as Figure 6. The plasma inhomogeneities may be most easily seen by the spiky appearance of the energy fluxes above general background levels of 2 x 10^{10} cm^{-2} sr^{-1} s^{-1} eV^{-1} in panel 5. Good examples are noted by arrows in panel 5 at 0508 UT, 0512 UT, 0529 UT, 0532 UT, and 0533 UT. (The large electric bipolar pulse at 0515 UT does not correspond to a plasma inhomogeneity as defined here and has a different cause, as explained below.)

Figure 7

Generally, in the mixing region, the low energy electrons have a strong parallel anisotropy with balanced number fluxes, while the higher energy electrons have a trapped population (Figure 7, panels 6 and 4). These features are a strong indication that this plasma resides on closed field lines (*Ogilvie et al.*, 1984, *Fujimoto et al.,* 1998a, b).

Further fine structure is evident in the mixing region. Whereas inside the plasma inhomogeneities the high energy component is enhanced, there are instances when the reverse is the case and the low energy electron component is enhanced instead. Good examples are noted by the arrows at the top of Figure 7 at 0507 UT, 0515 UT and ~0522-0524 UT. They refer to enhancements antiparallel to the ambient field (panels 1 and 6 in Figure 7). We shall discuss the 0515 UT example, which is related to the large (10mV/m) electric pulse (Figure 4), also in relation to the aurora below (section 5.2).

The mixing region ends at 0534 UT, after which the electron and ion populations are more homogeneous and the average energy rises to 6-7 keV (ions) and 4 keV (electrons; Figure 4). These properties characterize the central plasma sheet (CPS) population, and from the magnetic field plot (Figure 3) this is the region where the periodic oscillations occur. CPS precipitation is thus the source of the R2 current system on this pass. We note that Polar crossed the R1/R2 boundary (at 0534 UT) when the time-lagged IMF started a prolonged southward rotation (4th vertical guideline in Figure 2).

5. Ground-based Observations

5.1 IMAGE Magnetograms at Svalbard

Figure 8a shows the X-component of the ground magnetic field observed at 5 stations in the Svalbard archipelago for the interval 0400-0600 UT plotted at 10 s resolution. The data are shown with the average over the interval subtracted out. Positive X is in the direction of geographic north. In the simplest approximation (spatially uniform, stationary, Hall current density in a sheet of infinite spatial extent) the X-component of the geomagnetic perturbation is proportional to the east-west component of the ionospheric Hall current (east – positive X deflection) and to the east-west component of the ionospheric **E** x **B** plasma drift (west – positive X deflection; e.g., *Fukushima*, 1969). The ILTs of the stations are given near the station designation. They decrease from top to bottom and range from 75.8° (NAL) and 71.4° (BJN). With the latitudinal extent of the large-scale currents inferred from Polar and depicted in Figure 1, we expect NAL and LYR to be beneath the R1 current and HOR, HOP and probably also BJN to be underneath the R2 current.

Figure 8a

We make two points. First, a large-amplitude bipolar signature occurs between 0510 - 0515 UT (bracketed by the vertical guidelines), whose phase reverses at station HOP, where its amplitude also maximizes. As explained below, a discrete auroral arc is related to this feature. Second, there are quasi-periodic oscillations at station HOP during 0515–0550 UT. These are related to oscillations of similar period in the R2 current at Polar from 0525 UT onwards. In Figure 8b and 8c we plot the power spectral

Figure 8b an

densities of the horizontal field disturbance (H) at HOP and the field disturbance perpendicular to the background field ($B_\perp$) at Polar, both for the interval 0534-0550 UT when Polar's footprint was close to station HOP (Figure 1) and, simultaneously, periodic oscillations were seen at both sites. A prominent peak at ~2.1 mHz (~8 min period) is evident in both spectra. If the power peak at HOP is taken together with the fact that at this ground station there is a phase change with respect to the neighbouring stations HOR and BJN, where the amplitude is also less, we may conclude that there is a field line resonance centered at the L-shell corresponding to that of HOP.

5.2 Optical Observations: Pulsing Aurorae

MSP plots and auroral images are available for 0515-0600 UT. Thus they are available during Polar's traversal of the R1 and R2 currents, but they are missing during Polar's passage through the C1 and C2 currents. Clear limitations on the analysis result from this which we need to bear in mind. In general, there are limitations inherent in the use of single-spacecraft data, which makes it difficult to distinguish between temporal and spatial variations. The lack of simultaneous data while Polar is in C1 and C2 implies that we cannot establish directly a 1-1 correspondence between these currents and any associated aurorae. We can only infer a possible relation using a fortunate circumstance, to which we have alluded already, namely, the similarity of the IMF and solar wind parameters when Polar is crossing C1 in interval I and when the ground instruments are acquiring data in interval IV pertaining to the same latitude range where the footprint of POLAR maps to during its traversal of C1 (see Figure 1).

MSP plots for the interval 0525 – 0600 UT are shown for the red and green line emissions in Figures 9a and 9b, respectively. Line-of-sight intensities are plotted versus zenith angle from 70° north of zenith (NZ) to 70° SZ, color-coded as in the bar underneath each plot. Four latitudinally separate auroral forms may be seen. An aurora entending from 30 to 65 NZ in the red line persists throughout the entire interval. It is associated with emissions in both the red and green lines, whose intensities vary manifestly in time. Major brightenings occur around 0545 UT and 0552 UT and may be associated with the more southerly directed IMF within interval IV.

Figures 9a a

Two bands of emission lie equatorward of this major form in the north. They light up first at ~0545 UT at 20 NZ and 10-20 SZ, respectively, intensify sporadically in the rest of the interval shown, notably at 0550 UT, and 0553 UT, as they follow a parallel equatorward migration. Equatorward of 30 SZ, a fourth, much more diffuse emission is present in the green line (Figure 9b). The intensity of this emission, too, appears to be modulated, but at a lower frequency than the other auroral forms. In the interval shown one can make out 5-6 intensifications (indicated by arrows), implying an average periodicity of 7-8 min. This emission also advances equatorward, reaching the southern edge of the field of view by the end of the interval considered.

These four latitudinally separate bands of auroral emission can be related to (a) the large-scale currents shown in Figure 3, (b) the electric field behavior (Figure 4), and (c) the plasma regimes observed by Polar (Figures 5 – 7). We start with the intervals where joint auroral-Polar observations are available, discussing first the Polar-Svalbard conjunction during the interval 0515-0534 UT, when Polar is in R1. Representative

of the auroral observations in this interval is the ASC sequence at 630.0 nm shown in Figure 10 taken during the period 0516-0521 UT. The dotted white line through MN (magnetic north) gives the scanning direction of the MSP. The ASC captures two major forms fanning out in the magnetic east direction. These are midmorning east-west aligned arcs. They correspond to the time when Polar is in the R1 current, as indicated in Figure 1, with its footprint traversing the equatorward arc. During this 5-min period the auroral luminosity intensifies during 0516-0518 UT and fades slightly afterwards. Figure 10

The equatorward arc is traversed by Polar at ~0515 UT when Polar/HYDRA observed a strong intensification of low energy electrons (Figure 5), Polar/EF observed a strong bipolar electric signature (Figure 4), and the Svalbard magnetometers recorded a strong magnetic perturbation (Figure 8a). The interval 0510 – 0515 UT is marked in Figure 8a. The strongest perturbation at 0515 UT is at LYR and HOR which bracket the equatorward arc. We show a green line representation of the aurora corresponding to this current element at 0515 UT in the R1 current in Figure 11. Green line ASC observations of the same arcs as in Figure 10 straddling the zenith of the station in the east-west direction are easily identified. Whereas images 1 and 6 show two weak arcs, during 0516-0518 UT, i.e., starting 1 min after the electric field signature was seen by Polar, a brightening of both arcs occurs, particularly evident in the 0516:45 UT image. Local to the mapping of Polar, a brightening in the equatorward arc is seen in Figure 11 in the 0516:15 UT and 0516:45 UT images. Locally, therefore, more precipitation is being fed to the aurora through an activation of small-scale current elements embedded within the downward region 1 current. Consistent with the electric field variations Figure 11

in Figure 4, the arc at 0515 UT is embedded in R1 while the poleward arc could be associated with the convection reversal seen there at 0505 UT. Note the enhancement in electrons between 0506 and 0507 UT in Figure 7.

We next consider the southernmost, diffuse aurora when the Polar footprint lies in the southeastern part of the ASC field of view (Figure 1). From 0534 UT to 0600 UT, Polar was in the R2 current and was observing CPS particles (Figures 3 and 5) traversing the latitudinal range of the diffuse green line aurora (Figure 9b). Thus this aurora corresponds to the R2 current system, and its source is CPS precipitation. In the interval 0534-0600 UT the meridian scanner sees 4 intensity maxima (arrows in Figure 9b). This ~8 min average recurrence period is comparable to the average periodicity of the POLAR/MFE regular oscillations (Figure 3, Figure 8c). The equatorward motion of this, as well as all the other auroral forms, is related to IMF conditions, with the southward turning at 0534-0540 UT (Figure 2) initiating the migration of the aurorae toward the equator.

At this point we would like to make a consistency check of our ground-space correspondencies. The observations at time 0534 UT afford an excellent opportunity for doing so. At 0534 UT, the MSP plot of Figure 9b shows that the diffuse aurora (green line panel) extends up to 15 SZ, which corresponds to 75° ILT. At 0534 UT Polar sees a transition from R1 (BPS) to R2 (CPS) at 75.4 ILT. At 0534 UT, the aurora sees this boundary as well in the form of a transition from the multiple arcs to the diffuse aurora at 75 ILT. This shows the consistency of the coordinate systems.

Reasonable associations can be made between the aurora and current regimes prior

to the time when twin-site data are simultaneously available. Poleward of the aurorae just discussed are other emissions and, correspondingly, another current system north of R1 (C1 + C2). Recall from the Introduction that this aurora is observed under very similar interplanetary conditions as those in interval I (see Figure 2). We shall thus compare the ground observations of this aurora made in interval IV with particle observations made in the same latitude region by Polar in interval I, recognizing that an exact comparison is impossible. Rather, we will consider representative characterisitics that may be plausible. Figure 1 shows the ILT regime where this aurora is observed, which is similar to the ILT span of the mapped Polar orbit at this time. It thus seems reasonable to conclude that the northernmost aurora in Figure 9a should correspond to the cleft current system C1+C2 in Figure 3. For this reason it has been marked "cusp aurora" in Figure 1. The cusp aurora is characterized by episodic brightenings in both the red and green emissions. During the time of the equatorward migration (0540 - 0600 UT), there are 5 brightenings (Figure 9b), corresponding to an average periodicity of $\sim$5 min. This is a similar periodicity to that of the ion bursts seen by Polar in the C1 current.

We now zoom in on the two-dimensional aspects of this aurora by showing the period 0540 - 0555 UT in Figure 12. This period is associated with the strong brightening of this poleward aurora mentioned earlier when discussing the MSP (Figures 9a, b). Visually, one can distinguish two types of emission, particularly after the brightening at 0546 UT. There are first two east-west aligned forms, limited in latitudinal extent, which straddle zenith and belong to the R1 current described above. There is then

a form to the north of these, likewise elongated generally east-west, but occupying a broader range of zenith angles. This zenith angle spread is in part due to the altitude distribution of the emission, which takes the form of rays, as is typical of the cusp region. As noted already when discussing the MSP data, this latter aurora visibly intensifies between 0549-0555 UT (lower row of panels) when the IMF clock angle exceeds 135° (Figure 2). A video sequence of this aurora strongly indicates that the auroral rays in the highest latitude form move westward (antisunward) whereas the lower discrete arcs to the south move eastward (sunward). This indicates that a convection reversal exists between the latitudes of the cusp type emission and the discrete forms to the south of it. This inference is consistent with the electric field observations from Polar around 0505 UT (Figure 4) when the spacecraft crossed a convection reversal close to our designated interface between the C2 and R1 currents (section 4.1.) This confirms that the various observations at the two heights have been properly interpreted.

The positions of the aurorae relative to the current systems observed by Polar, and their motions, at two times (0530 UT and 0555 UT) are shown in Figure 13, displayed in a polar plot of MLAT versus MLT. The top schematic shows the Polar footprint (thin arrowed line) directed south, on which are marked the current systems C1, C2, R1 and R2 and the direction of current flow (a solid circle indicates current out of the ionosphere). To the right of the trajectory and on the direction of the meridian scanner are noted the corresponding aurorae, labeled A-C. The Polar footprint at 0530 UT is indicated by an 'X' symbol in R1 close to the R1/R2 interface. Type A is the cusp-type aurora, type B is the multiple discrete forms, and type C is the diffuse aurora.

Figure 13

The direction of motion of the forms is shown in the bottom schematic, referring to 0555 UT. At this time Polar's footprint is near the southern edge of the field of view in the type C aurora whose source is the CPS and which is moving sunward. The ground instruments observe at this time the type A (cusp-type) aurora which periodically intensifies and expands westward (antisunward). As inferred from the ASC, this aurora extends from the eastern edge of the field of view without reaching the western edge, as indicated. Motion in the type B arcs is generally in the eastward (sunward) direction, as shown by the arrows.

Discussion

6.1 Summary of the observations

We related observations of large-scale magnetospheric current systems and their temporal variations made by Polar with likewise temporarily varying aurorae observed from Svalbard, Norway, when the magnetic footprint of the spacecraft crossed the field-of-view of the ground instruments on December 3, 1997. We emphasize that some of the associations with the aurora (after 0515 UT) were obtained by direct comparison of the twin-site observations, and some (before 0515 UT) were inferred indirectly using data taken at a separation of 1 hour. On the latter point, the reader may gauge the reasonableness of comparing the *in situ* and ground-based data sets from the following points: (i) Polar traversed the regime of cusp FAC/pulsed plasma injection in the same latitude range in which the cusp aurora was observed from the ground 1 hour later (see

Figure 1 for the correspondence); (ii) these two intervals (i.e., Polar's cusp traversal in interval I and the ground observations of the cusp in interval IV) were characterized by very similar IMF conditions; (iii) the periodicity of Polar's cusp plasma injections is similar to that of the brightenings in the cusp aurora; and (iv) ASC data show that the northernmost auroral forms are cusp-type (long rays), contrary to the discrete arcs on its equatorward side, near zenith (those related to R1).

The conjunction we discussed took place in the ∼0900 MLT sector at 80.5°–73.3° ILT. We combined the *in situ* observations of plasma, and magnetic and electric fields with meridian scanning photometry and all-sky imagery from the ground site and magnetograms from stations at Svalbard. Descending in altitude from ∼7.5 to ∼5.5 R_E on a southbound trajectory, Polar traversed a four-sheet current system: a twin-sheet cusp-type current system C1-C2, spanning the ILT range 80.6°–77.7°, and then the traditional regions 1 (R1) and 2 (R2) current pair, extending from 77.7° to 73.3° ILT. Currents in C1 and R2 are flowing out of the ionosphere; those in C2 and R1 are directed into the ionosphere. It is stressed that the association of current regimes and their boundaries were not inferred from the magnetometer alone, but from the full complement of instruments on Polar, which included measurements of particles (ions and electrons) and electric fields.

Within C1, Polar observed bursts of ions of typically magnetosheath energies, repeating at ∼5 min intervals, each burst causing localized perturbations in the magnetic field. Intensified field-aligned electron beams accompanied the ion bursts. These are being observed downstream of the cusp along the 0900 MLT meridian, i.e., the plasma

mantle. We infer this from (i) the MLT and ILT location, which agrees with statistical maps of mantle precipitation at low altitudes (*Newell and Meng*, 1992, their Figure 1), and (ii) its location on upward-flowing current when IMF $B_y > 0$, which agrees, in turn, with theory (see *Lee et al.*, 1985, their Figures 2 and 3). The ground-based auroral observations made later but pertaining to the same latitude range as the C1 current and to similar IMF conditions as when the C1 current was crossed by Polar, suggest a cusp-type aurora which is also characterized by episodic brightenings in both red and green emissions. The periodicity of these brightenings matches that of the plasma bursts at Polar. Within C2, when the IMF clock angle had decreased to an average value of 60°, the pulsing ceased, but magnetosheath plasma was still present, only at diminished intensity.

A mixing region of magnetosheath and magnetospheric plasmas with spectral characteristics of the BPS formed the source of the R1 current. On December 3, 1997, there was evidence of fine structure: (i) plasma inhomogeneities, where the magnetospheric component was relatively enhanced; and (ii) bipolar current elements, where instead the magnetosheath component was relatively enhanced. These small-scale features are related to east-west aligned, discrete forms in the aurora, sometimes called "fan" arcs (*Meng and Lundin*, 1986). Item (i) was also present in a previous conjunction on November 30, 1997, and there, as here, these plasma inhomgeneities are sources of the east-west aligned arcs.

In the later part of the event after ~0540 UT both discrete and diffuse aurorae advanced steadily equatorward as the IMF rotated steadily south. This is thus clearly a

temporal change. Their intensity was strongly modulated in association with enhanced IMF southward turnings. Within R2, when Polar was sampling the central plasma sheet, a field line resonance was observed on Polar and the underlying ground station HOP. The corresponding, diffuse green line aurora was also pulsed and both these auroral and magnetic pulsations are in the Pc 5 range ($\sim$2.1 mHz).

A note is in order here about the dispersionless character of the ion bursts observed by Polar in the C1 current (mantle precipitation). There are various possible reasons. The first is that the injections are local. In this case ions of different energies have no time to separate. The second is the converse of this, i.e., they are injected so far away that the higher energetic particles never crossed the path of Polar, and we are looking at the lower energy tail of a time-varying process. The third is that of a sequence of reconnected flux tubes passing over the spacecraft. The velocity of the spacecraft is much less than that of the flux tubes, so that it hardly moves at all during the observation. If we assume the same reconnection site for all flux tubes, the spacecraft will intersect them after an equal length of time has elapsed since they were formed by reconnection. In that case, no spatial dispersion occurs.

The first case is not tenable on *Taguchi et al.*'s model, to which we wish to specifically compare the observations (see below). In that model the high-latitude C1 current is formed by flux tubes reconnected at higher latitude "end" of the reconnection line in the post-noon sector which are convected antisunward and dawnward by field-line tensions appropriate to a $B_y > 0$ IMF. The present observation is, however, on the pre-noon side. The third case, which is the one we favor, is plausible because Polar only

covers $\sim$1.1° ILT in the C1 current. However, with the data to hand it is impssible to exclude the second case.

We now address two aspects of this study: (1) interpretation of the observations in terms of time varying reconnection; (2) regulation of M-I coupling at 0900 MLT by IMF B_y and B_z.

Interpretation in Terms of time-varying reconnection

As interpretational scheme we use the conceptual model of *Taguchi et al.* (1993) but extend it to include time variability, as warranted by our observations. (Short duration variations were noted in that work but not investigated further.) We then discuss the new elements here, namely the pulsing behavior in plasmas and aurorae. Taguchi et al. show how positive IMF B_y is responsible for the directions of the C1 and C2 currents (which are termed in that work HCC and LCC, for high (low) cleft currents; see also *Ohtani et al.* (1995)). They show that in all cases with $B_y > 0$ (in fact, by their selection criteria, > 5 nT), the poleward member of the cusp current sheets had upward current and the equatorward member had downward current. (The reverse directions result for strongly negative B_y). These current directions also result from theoretical arguments (*Lee et al.*, 1985). Taguchi et al. attribute the cleft precipitation to open field lines that thread the magnetopause. Their model assumes a reconnection line at the magnetopause which, for positive IMF B_y, is inclined with its pre-noon side at low latitudes and its post-noon side at high latitudes (*Gonzalez and Moser*, 1974; *Cowley*, 1981). They consider the motion of bundles of field lines reconnected at its pre-

and post-noon sides. Subsequent to reconnection, all field lines move tailward under a combination of magnetic tension forces and drag by the magnetosheath flow. Figure 14 reproduces their schematic model showing the motion of the open field lines after reconnection under IMF $B_y > 0$. Under the different directions of the magnetosheath flow at the two "ends" of the reconnection line, the field lines reconnected post-noon will convect to higher latitudes than those reconnected pre-noon. The plasma flows through the rotational discontinuity magnetopause across the magnetic field, giving rise to an electric field (open arrows in the figure). The region where this electric field acts (hatched area) forms the source region of the cusp/cleft currents. The electric field is transmitted down the magnetic field lines to the ionosphere and, as a result, an approximately poleward-directed electric field appears in the ionosphere (see lower diagram in Figure 14). The Pedersen currents driven by this electric field form the closure current in the ionosphere for the C1/C2 FACs.

Figure 14

Various features of our observations are consistent with model predictions. These concern (1) the presence of 4 FACs in the pre-noon sector for IMF $B_y > 0$; (2) the direction of C1 (out of the ionosphere) and C2 (into the ionosphere) for IMF $B_y > 0$; (3) invariant latitude location ($\sim$77°-80°); and (4) C1/C2 as a current sheet contiguous with, but independent of, R1/R2. We established the latter point from observations: (i) the different character of the magnetic fluctuations; (ii) plasma characteristics different from neighbouring regimes; (iii) the presence of a convection reversal; (iv) Association of a distinct aurorae. (5) The C1/C2 system was also found in our case to lie on generally tailward flowing plasma – the convection reversal was at the C2/R1 interface

– as would also result from this model. Concerning the MLT location (0900 MLT), ours corresponds to the most dawnward C1 seen in Taguchi et al.'s examples under $B_y > 0$ (see their figure 6a).

New elements are introduced into this picture by the time variability on December 3, 1997. (1) In C1, we find evidence of pulsed plasma transfer, with an intensified magnetosheath ion population occurring in bursts which repeat every ∼5 min. These pulses were observed in C1 when the IMF pointed strongly south, and were accompanied by perturbations in the local field components. On the reconnection interpretation, these pulses of enhanced magnetosheath particles would correspond to enhancements in the reconnection rate. The electrons were bidirectionally streaming. Electrons counterstreaming along the magnetic field in flux transfer events (*Russell and Elphic*, 1978), which are signatures of time-dependent reconnection, have been observed before (*Scudder et al.*, 1984; *Farrugia et al.*, 1988). The electrons emanating from the X-line or the magnetosheath move rapidly along the field lines, and those moving away from Earth have already been mirrored close to Earth.

(2) In C2, when the IMF was weakly northward (average clock angle ≈ 60°), the plasma pulsing stopped, but the magnetosheath plasma was still present though at diminished intensity. These observations would then correspond more closely to those of *Taguchi et al.* (1993). Taking into account a large body of studies of *in situ* observations of reconnection at the low latitude magnetopause, which confirm the continued presence of reconnection when the the magnetic shear across the magnetopause (a quantity which is approximately equal to the IMF clock angle at low magnetopause latitudes

[*Farrugia et al.*, 1998a]) is as low as 45° (*Phan et al.,* 1996), we hypothesize the continued presence of reconnection during the observations in C2. Nevertheless, it is still an unsolved issue why at low clock angles the inferred reconnection process should become steady. A significant topological change might have occurred when the field directional discontinuity, at which the IMF turned sharply north, arrived, as discussed in an analogous context by *Maynard et al.* [2001].

(3) A novel point was our association of an aurora with the cleft/cusp currents. This consisted of an emission at comparable ILATs to the HCC inferred from statistics by Taguchi et al., i.e., within 77 - 80°. The aurora which we associated with the cleft current system traversed by Polar earlier was observed to be also subject to temporal variability, being strongly pulsed in both the red and green lines. We propose therefore that this is the auroral signature of the pulsed plasma transfer due to reconnection. Furthermore, this aurora brightens strongly in association with southward IMF turnings, further supporting its association with the time-varying reconnection process.

The suggested association between Polar plasma/field observations in interval I (centered around 0430 UT) and the ground observations of the cusp-type aurora in interval IV (centered around 0550 UT) is quite reasonable since these two observations refer to the same magnetospheric position/field line (approximately 0900 MLT/77-80 ILT) and very similar IMF conditions. The absence of cusp-type aurora in Figure 10, representing approximately 0518 UT, when the IMF was oriented eastward with $B_z \approx 0$ (interval III), is reasonable in view of the strong IMF regulation of the cusp longitudinal and latitudinal extent (see e.g. *Crooker*, 1991, *Maynard et al.*, 1997, *Farrugia et al.*,

1998b). The present observation is, in fact, an illustration of the IMF regulation of the cusp.

Regulation of M-I Coupling at 0900 MLT by the IMF components

The observations indicate regulation of magnetosphere-ionosphere coupling at 0900 MLT by the IMF. These are temporal effects, which we believe are modulating the underlying spatial structure. First, the strong impact of IMF B_z may be seen both in the cusp aurora and in the multiple arcs. They drift southward and intensify during steady southward rotations of the IMF and enhanced southward turnings. Secondly, the pulsed plasma observed at Polar between 0412 UT and 0447 UT occurs, as we have seen, when the IMF clock angle is large, to which both B_z and B_y contribute. The periodicity of the plasma bursts is similar to that of FTEs ($\sim$5 min) and lends further support to our interpretation that the plasma bursts are signatures of temporal structure in the reconnection process. Finally, we note that the times of the changing of the FAC/plasma regimes by Polar often occurred at times when IMF changes took place. Thus the timings of the crossings of the C1/C2, and R1/R2 interfaces by Polar coincide very well with the timings of changes in IMF B_z polarity. A northward turning of the IMF decreases the merging rate. A small inflation of the magnetosphere could be expected, which could move the C1 region outside of Polar.

This last issue is closely related to the temporal/spatial aspects of the conjunction. With one spacecraft it is difficult, if not impossible, to unambiguously separate the two. Both aspects are present. When the configuration reacts to changes in the IMF, there is

a response function involved, as many past studies have shown. We took this implicitly into account when we obtained the lag time for the IMF to influence the ionosphere, adding several minutes to the nominal convection time. We also considered that the propagation delay time may vary, as shown by *Weimer et al.* [2002]. We obtained this extra delay time by aligning the period of intense, pulsed, magnetosheath plasma C1 with IMF interval I, when the IMF has a persistent southward component. Its relatively abrupt termination then coincides with the abrupt northward turning of the IMF. We retained this delay throughout, effectively assuming a constant response time of the whole configuration. The same correlation time with the IMF places the subsequent southward turning near the R1/R2 boundary. This boundary is known to be a spatial one from decades of previous measurements. The fact that we cross it when B_z turns southward appears to be by chance, but may be related to the stronger merging at the magnetopause and its impact on magnetosphere dynamics.

Acknowlegements

We thank the referees for their many helpful comments. We are grateful to Jack Scudder for helpful discussions and use of Polar/HYDRA data. We are indebted to K. W. Ogilvie and R. P. Lepping for providing us with key parameter data from the SWE instrument and 3 s resolution data from the MFI instrument on Wind, respectively, and to Christopher T. Russell for providing us with Polar/MFE high resolution magnetic field data. We are also grateful to A. Viljanen and the German-Finnish-Norwegian-Polish IMAGE project team lead by the Technical University of Braunschweig for Scandinavian

magnetometer data (http://www.geo.fmi.fi/image/index.html). This work is supported by NASA Living with a Star grants NAG5-121189 and NAG5-10883, and NASA grants NAG5-11676, NAG 5 - 11803. The optical observations at Ny-Ålesund are supported by the Norwegian Polar Research Institute, the Kings Bay Coal Company, and AFRL, the Norwegian Research Council. NCN and DMO acknowledge support from the NASA Polar Program through subcontract with the University of California, Berkeley, and from AFOSR Task 2311AS.

References

Armstrong, J. C., and A. J. Zmuda, Triaxial magnetic measurements of field-aligned currents at 800 km in the auroral region: Initial results, *J. Geophys. Res., 78*, 6802, 1973.

Cowley, S. W. H., Magnetospheric asymmetries associated with the Y-component of the IMF, *Planet. Space Sci., 29,* 79, 1981.

Crooker, N. U., F. R. Toffoletto, and M. S. Gussenhoven, Opening the cusp, *J. Geophys. Res., 96,* 3497, 1991.

Doyle, M. A., F. J. Rich, W. J. Burke, and M. Smiddy, Field-aligned currents and electric fields observed in the region of the dayside cusp, *J. Geophys. Res., 86,* 5656, 1981.

Erlandson, R. E., L. J. Zanetti, T. A. Potemra, P. F. Bythrow, and R. Lundin, IMF B_y dependence of region 1 Birkeland currents near noon, *J. Geophys. Res., 93*, 9804, 1988.

Escoubet, C. P., M. F. Smith, S. F. Fung, P. C. Anderson, R. A. Hoffman, E. M. BAsinska, and J. M. Bosqued, Staircase ion signature in the polar cusp: A case study, *Geophys. Res. Lett., 19,* 1735, 1992.

Farrugia, C. J., R. P. Rijnbeek, M. A. Saunders, D. J. Southwood, D. J. Rodgers, M. F. Smith, C. P. Chaloner, D. S. Hall, P. J. Christiansen, and L. J. C. Wooliscroft, A multi-instrument study of flux transfer event structure, *J. Geophys. Res., 93,* 14,465, 1988.

Farrugia, C. J., F. T. Gratton, L. Bender, H. K. Biernat, N. V. Erkaev, J. M. Quinn, R. B. Torbert, and V. V. Dennisenko, Charts of joint Kelvin-Helmholtz and Rayleigh-Taylor instabilities at the dayside magnetopause for northward IMF, *J.Geophys. Res., 103*, 6703, 1998a.

Farrugia, C. J., Sandholt, P. E., J. Moen, and R. L. Arnoldy, Unusual features of the January 1997 magnetic cloud and their effect on optical dayside auroral signatures, *Goephys. Res. Lett., 25,* 3051, 1998b.

Farrugia, C. J., P. E. Sandholt, N. C. Maynard, W. J. Burke, J. D. Scudder, D. M. Ober, J. Moen, and C. T. Russell, Pulsating midmorning auroral arcs, filamentation of a mixing region in a flank boundary layer, and ULF waves observed during a Polar-Svalbard conjunction, *J. Geophys. Res., 105,* 27,531, 2000.

Fujimoto, M., T. Mukai, H. Kawano, M. Nakamura, A. Nishida, Y. Saito, T. Yamamoto, and S. Kokubun, Structure of the low-latitude boundary layer: A case study with Geotail data, *J. Geophys. Res., 103,* 2297, 1998a

Fujimoto, M., T. Teresawa, T. Mukai, Y. Saito, T. Yamamoto, and S. Kokubun,

Plasma entry from the flanks of the near-Earth magnetotail: Geotail observations, *J. Geophys. Res., 103,* 4391, 1998b.

Fukushima, N., Equivalence in ground geomagnetic effect of Chapman-Vestine's and Birkeland-Alfven's electric current-systems for polar magnetic storms, *Rep. Ionosph. Space Res. Japan*, 23, 1969.

Gonzalez, W. D., and F. S. Mozer, A quantitative model for the potential resulting from reconnection with an arbitrary interplanetary magnetic field, *J. Geophys. Res., 79,* 4186, 1974.

Harvey, P., F.S. Mozer, D. Pankow, J. Wygant, N.C. Maynard, H. Singer, W. Sullivan, P.B. Anderson, R. Pfaff, T. Aggson, A. Pedersen, C.-G. Fälthammer, and P. Tanskanen, The electric field instrument on the Polar spacecraft, *Space Sci. Rev., 71*, 583, 1995.

Iijima, T., and T. A. Potemra, Field-aligned currents in the dayside cusp observed by TRIAD, *J. Geophys. Res., 81,* 5971, 1976.

Lee, L. C., J. R. Kan, and S.-I. Akasofu, On the origin of cusp field-aligned currents, *J. Geophys. 57*, 217, 1985.

Lepping, R.P., M.H. Acuna, L.F. Burlaga, W.M. Farrell, J.A. Slavin, K.H. Schatten, F. Mariani, N.F.Ness, F.M. Neubauer, Y.C. Whang, J.B. Byrnes, R.S. Kennon, P.V. Panetta, J. Scheifele, and E.M. Worley, The Wind Magnetic Field Investigation, *Space Sci. Rev., 71*, 207, 1995.

Lockwood, M., and M. F. Smith, The variation of reconnection rate at the dayside magnetopause and cusp ion precipitation, *J. Geophys. Res., 97,* 14,841, 1992.

Lühr, H., The IMAGE magnetometer network, *STEP Int., 4*(10), 4, 1994.

Maynard, N. C., T. L. Aggson, E. M. Basinska, W. J. Burke, P. Craven, W. K. Peterson, M. Sugiura, and D. R. Weimer, Magnetospheric boundary dynamics: DE 1 and DE 2 observations near the magnetopause and cusp, *J. Geophys. Res., 96*, 3505, 1991.

Maynard, N.C., E. J. Weber, D. R. Weimer, J. Moen, T. Onsager, R. A. Heelis, and A. Egeland, How wide in magnetic local time is the cups? An event study, *J. Geophys. Res., 102,* 4765, 1997.

Maynard, N. C., G. L. Siscoe, B. U. Ö. Sonnerup, W. W. White, K. D. Siebert, D. R. Weimer, G. M. Erickson, J. A. Schoendorf, D. M. Ober, and G. R. Wilson, Response of ionospheric convection to changes in the interplanetary magnetic field: lessons from a MHD simulation, *J. Geophys. Res., 106,* 21,429, 2001.

McDiarmid, I. B., J. R. Burrow, and M. D. Wilson, Magnetic field perturbations in the dayside cleft and their relationship to the IMF, *J. Geophys. Res., 83*, 5753, 1978.

Meng, C.-I., and R. Lundin, Auroral morphology of the midday oval, *J. Geophys. Res., 91,* 1572, 1986.

Newell, P. T., and C.-I. Meng, Mapping the dayside ionosphere to the magnetosphere according to particle precipitation characteristics, *Geophys. Res. Lett., 19,* 609, 1992.

Ogilvie, K. W., R. J. Fitzenreiter, and J. D. Scudder, Observations of electron beams in the low-latitude boundary layer, *J. Geophys. Res., 89,* 10,723, 1984.

Ogilvie, K.W., et al., SWE, A comprehensive plasma instrument for the Wind spacecraft, *Space Sci. Rev., 71*, 55, 1995.

Ohtani, S., T. A. Potemra, P. T. Newell, L. J. Zanetti, T. Iijima, M. Watanabe, L. G. Blomberg, R. D. Elphinstone, S. Murphree, M. Yamauchi, and J. Woch, Four large-scale field-aligned current systems in the dayside high-latitude region, *J. Geophys. Res., 100*, 137, 1995.

Phan, T.-D., G. Paschmann, and B. U. Ö. Sonnerup, Low-latitude dayside magnetopause and boundary layer for high magnetic shear, 2. Occurrence of magnetic reconnection, *J. Geophys. Res., 101,* 7817, 1996.

Russell, C. T., et al., The GGS/Polar Magnetic Fields Investigation, *Space Sci. Rev., 71*, 563, 1995.

Russell, C. T., and R. C. Elphic, Initial ISEE magnetometer results: Magnetopause observations, *Space Sci. Rev., 22,* 681, 1978.

Scudder, J. D., K. W. Ogilvie, and C. T. Russell, The relation of flux transfer events to magnetic reconnection, in *Magnetic Reconnection in Space and Laboratory Plasmas, Geophys. Monogr. Ser.*, vol. 30, p. 153, AGU, Washington, D. C., 1984.

Scudder, J., et al., Hydra - A 3-dimensional electron and ion hot plasma instrument for the Polar spacecraft of the GGS mission, *Space Sci. Rev., 71*, 459, 1995.

Sonnerup, B. U. O, and L. J. Cahill, Magnetopause structure and attitude from Explorer 12 observations, *J. Geophys. Res., 72,* 171, 1967.

Taguchi, S., M. Sugiura, J. D Winningham, and J. A. Slavin, Characterization of the IMF B_y-dependent field-aligned currents in the cleft region based on DE 2 observations, *J. Geophys. Res., 98,* 1393, 1993.

Tsyganenko, N. A., A magnetospheric magnetic field model with a warped tail

plasma sheet, *Planet. Space Sci., 37,* 5, 1989.

Weimer, D. R., D. M. Ober Ober, N. C. Maynard, W. J. Burke, M. R. Collier, D. J. McComas, N. F. Ness, and C. W. Smith, Variable time delays in the propagation of the interplanetary magnetic field, *J. Geophys. Res., 107,* paper 10.1029/2001JA009102, 2002.

Figure Captions

Figure 1.

A map showing the optical ground station at Ny-Ålesund, Svalbard, at the center of the field of view of the all-sky camera (ASC) for the red line (630 nm) aurora. The scanning plane of the photometer is shown by the double-arrowed line. The 76° magnetic latitude (= 75.8 invariant latitude, ILT) through the station is also shown. Polar's magnetic footprint is indicated, as are the projected extents of the large-scale current systems, C1, C2, R1 and R2.

Figure 2.

Wind/SWE and MFI data for the interval 0300 – 0700 UT, December 3, 1997. From top to bottom, the panels show the proton density, bulk speed, temperature, dynamic pressure, the total field and its GSM components, and the IMF clock and cone angles. The time has been shifted forward by 70 min, this being our estimated delay time for the IMF to affect Polar. Symbols I–IV designate the times Polar spends in large-scale current systems encountered during the conjunction.

Figure 3.

Polar/MFE magnetic field data at 6 s temporal resolution for the period 0400-0600 UT. Plotted are the GSM field components and the total field less the IGRF-1995 reference field. The extent of the large scale currents C1, C2, R1 and R2, identified from local measurements of fields and plasmas, are delimited by vertical guidelines.

Figure 4

Electric field data from Polar/EF for the period 0400 - 0600 UT. Shown the electric potential along the satellite track (top panel), and the electric field.

Figure 5.

Polar/HYDRA proton and electron observations for 0400-0600 UT, December 3, 1997. The top panel shows the ILT of the spacecraft. The two spectrograms display differential energy fluxes for ions and electrons, color-coded according to the respective color bars on the right. Then follow pitch angle-averaged energy and number fluxes integrated over energy, with electrons shown by a red trace.

Figure 6.

For the interval 0415 - 0505 UT, the panels show from top to bottom the differential energy fluxes of electrons flowing antiparallel ($J_{-\|}$), perpendicular ($J_{\perp}$), and parallel $J_{\|}$) to the magnetic field, the electron anisotropy $1/2(J_{\|} + J_{-\|})/J_{\perp}$ (log scale), the omnidirectional integral energy fluxes, and the integral number fluxes parallel (red) and antiparallel to the field.

Figure 7.

Electron behavior in the mixing region presented in the same format as Figure 6. Current elements are marked in the top panel. Examples of plasma inhomogeneities are marked in the fifth panel.

Figure 8a

X-component of the magnetic field at Svalbard ground stations for the period 0400 - 0600 UT. The average background field has been subtracted out.

Figure 8b, c:

Power spectral density of horizontal component of the magnetic field at station HOP (b) and the field fluctuations perpendicular to the background field ($B_\perp$) at Polar (c) during the time when Polar's magnetic footprint was closest to HOP. A spectral power peak at ~2.1 mHz is evident in both figures.

Figure 9.

Meridian scanning photometer (MSP) observations from Ny Ålesund during the interval 0525-0600 UT. The upper (a) and lower (b) panels show the red and green line emissions at 630.0 and 557.7 nm, respectively. Line of sight intensities are plotted as a function of zenith angle and time, color-coded according to the scales at the bottom of each panel. North is at the top.

Figure 10.

ASC images at 630.0 nm (1s integration time) for the interval 0516-0521 UT. The reference frame is zenith angle (30, 60 and 90° marked by dashed circles) and azimuth angle (geographic west (W) is up; south (S) is to the left). Ny Ålesund is in the center. The MSP scanning meridian is indicated by dashed line labeled MN (magnetic north).

Figure 11.

ASC images at 557.7 nm (1s integration time) taken at the following times: 0515:45, 0516:15, 0516:45, 0517:15, 0518:15, and 0518:45 UT. The format is the same as Figure 10.

Figure 12.

ASC images at 630.0 nm (2s integration time) taken at the following times: 05.40:00, 05.43:30, 05.46:01, 05.49:00, 05.52:00, and 05.55:00 UT. The format is the

same as in Figure 10.

Figure 13

The positions of the aurorae relative to the current systems observed by Polar, and their motions, at two times, 0530 UT and 0555 UT. For further details, see text.

Figure 14

A sketch illustrating the conceptual scheme proposed by *Taguchi et al.* (1993) to account for the presence of the cusp/cleft currents (reproduced from *Taguchi et al.*, 1993). The figure is drawn for positive IMF B_y.

POLAR Footprint, 12/03/1997

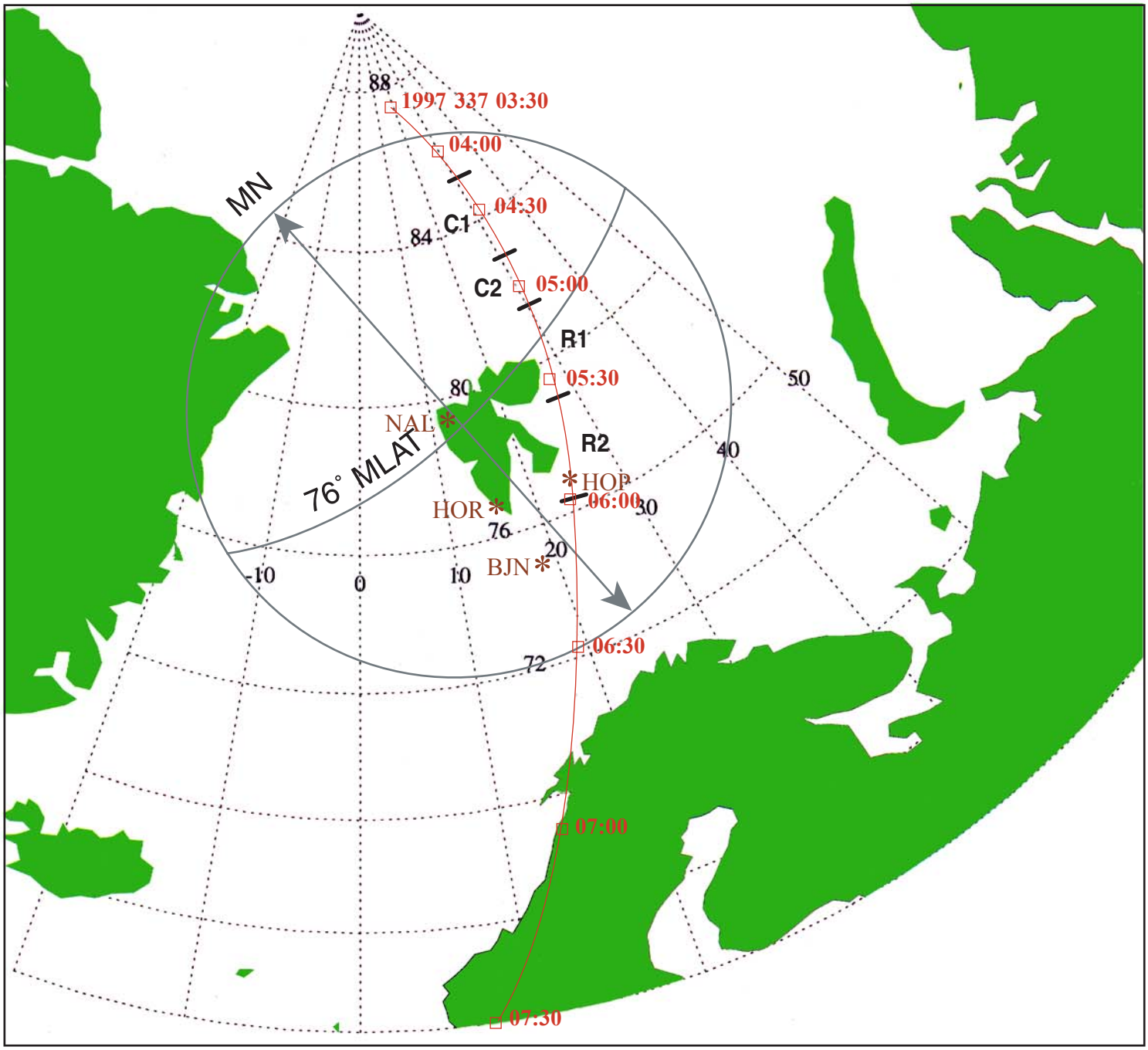

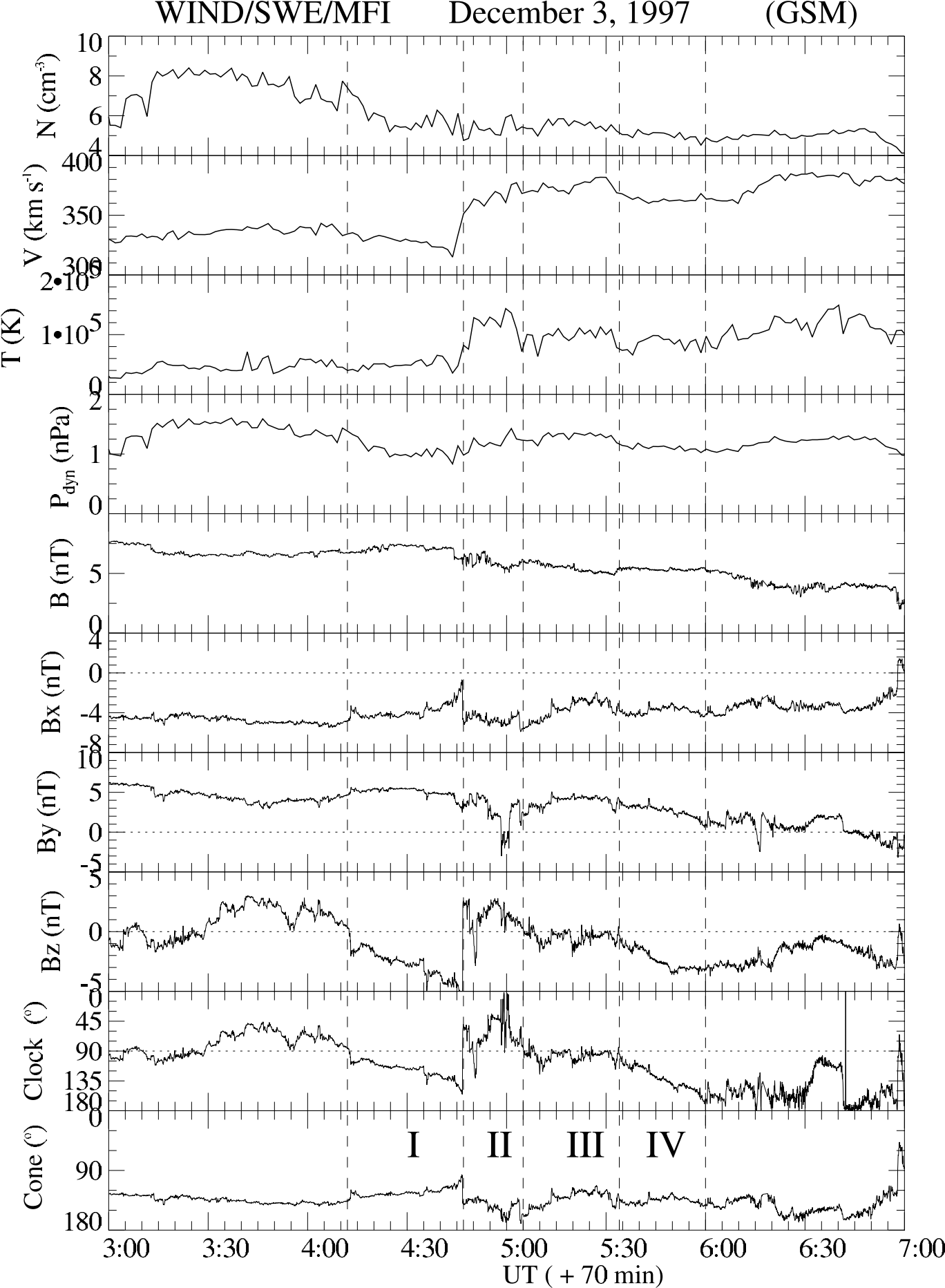
WIND/SWE/MFI December 3, 1997 (GSM)
N (cm-3)
V (km s-1)
T (K)
Pdyn (nPa)
B (nT)
Bx (nT)
By (nT)
Bz (nT)
Clock (°)
Cone (°)
I
II
III
IV
3:00
3:30
4:00
4:30
5:00
5:30
6:00
6:30
7:00
UT (+ 70 min)

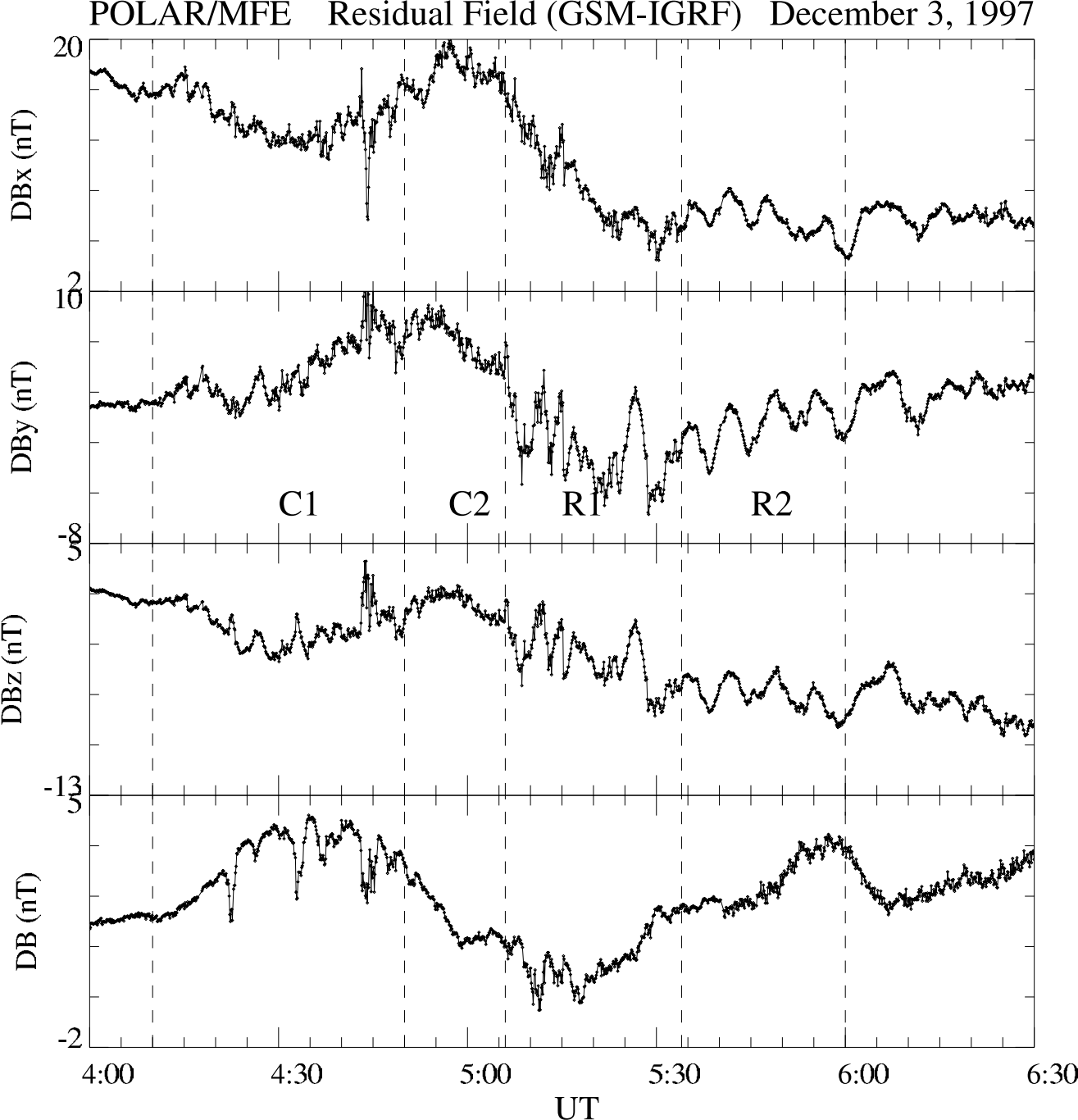
POLAR/MFE Residual Field (GSM-IGRF) December 3, 1997
DBx (nT)
20
2
DBy (nT)
10
-8
C1
C2
R1
R2
DBz (nT)
5
-13
DB (nT)
5
-2
4:00
4:30
5:00
5:30
6:00
6:30
UT

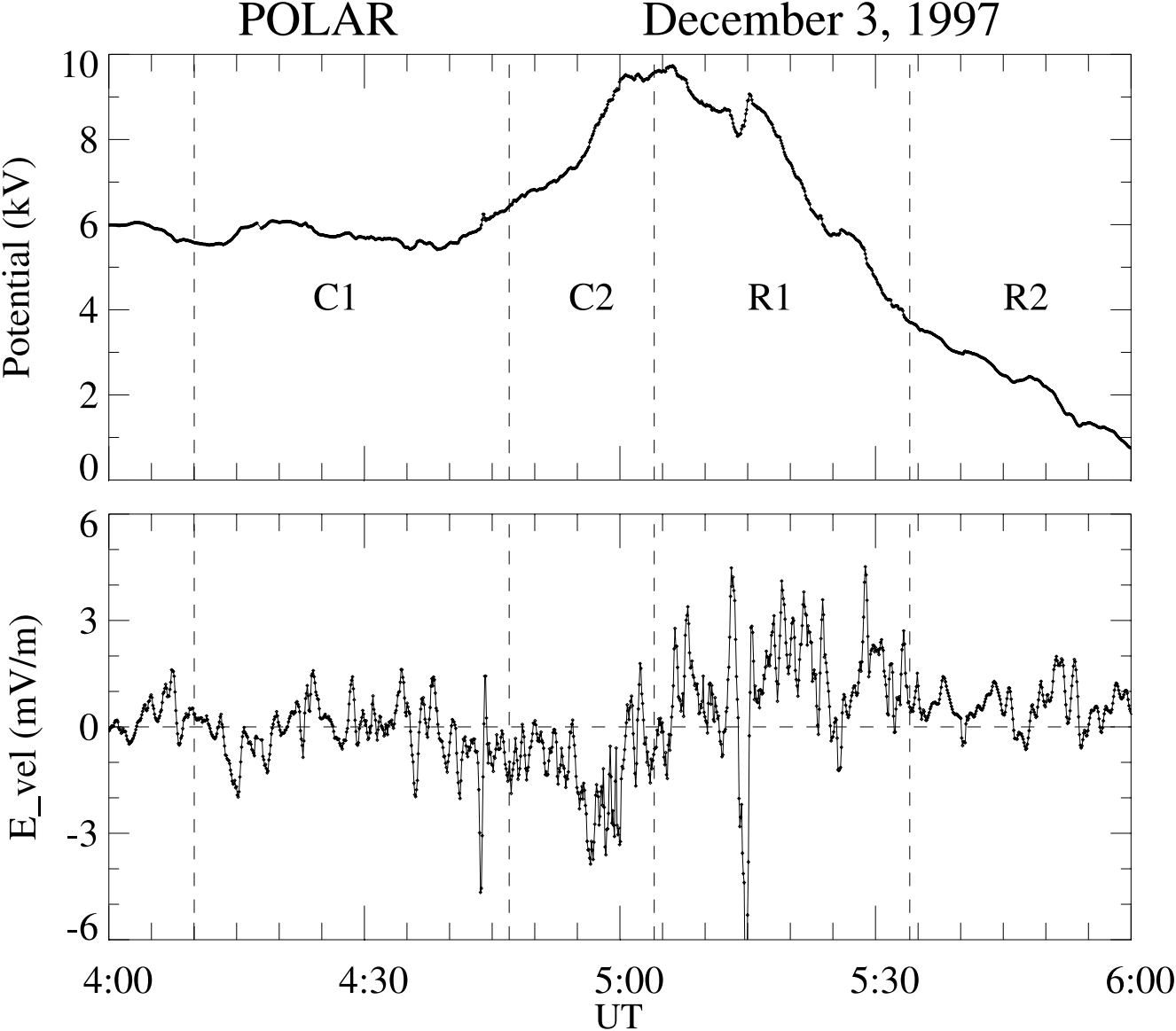
POLAR
December 3, 1997
Potential (kV)
10
8
6
4
2
0
C1
C2
R1
R2
E_vel (mV/m)
6
3
0
-3
-6
4:00
4:30
5:00
5:30
6:00
UT

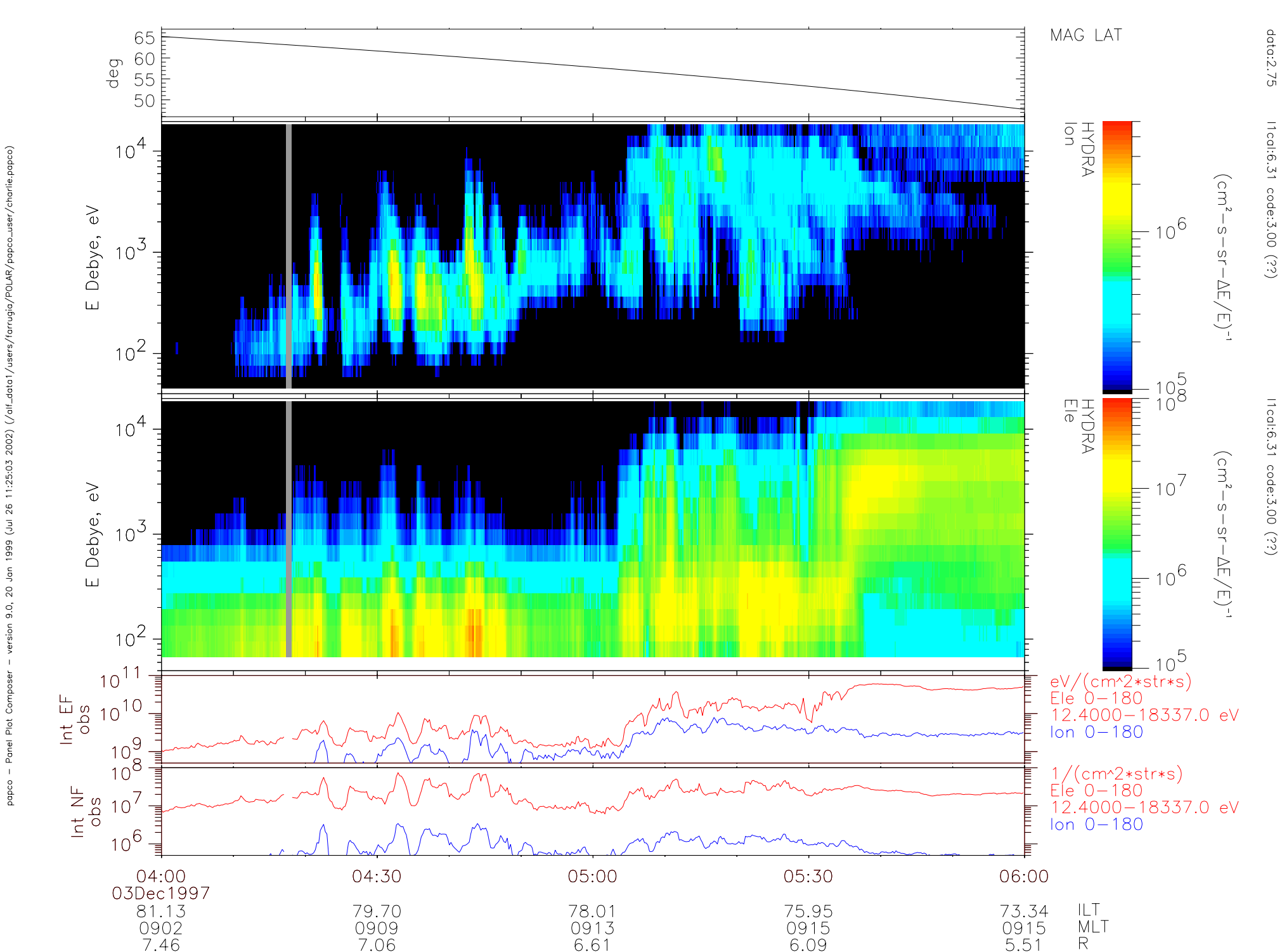
MAG LAT
deg
65
60
55
50
E Debye, eV
10^4
10^3
10^2
HYDRA
Ion
10^6
10^5
$(cm^2-s-sr-\Delta E/E)^{-1}$
HYDRA
Ele
10^7
10^6
10^5
Int EF
obs
10^{11}
10^{10}
10^9
eV/(cm^2*str*s)
Ele 0-180
12.4000-18337.0 eV
Ion 0-180
Int NF
obs
10^8
10^7
10^6
1/(cm^2*str*s)
Ele 0-180
12.4000-18337.0 eV
Ion 0-180
04:00
03Dec1997
04:30
05:00
05:30
06:00
81.13
0902
7.46
79.70
0909
7.06
78.01
0913
6.61
75.95
0915
6.09
73.34
0915
5.51
ILT
MLT
R
data:2.75
l1cal:6.31 code:3.00 (??)
l1cal:6.31 code:3.00 (??)
papco - Panel Plot Composer - version 9.0, 20 Jan 1999 (Jul 26 11:25:03 2002) (/alf_data1/users/farrugia/POLAR/papco_user/charlie.papco)

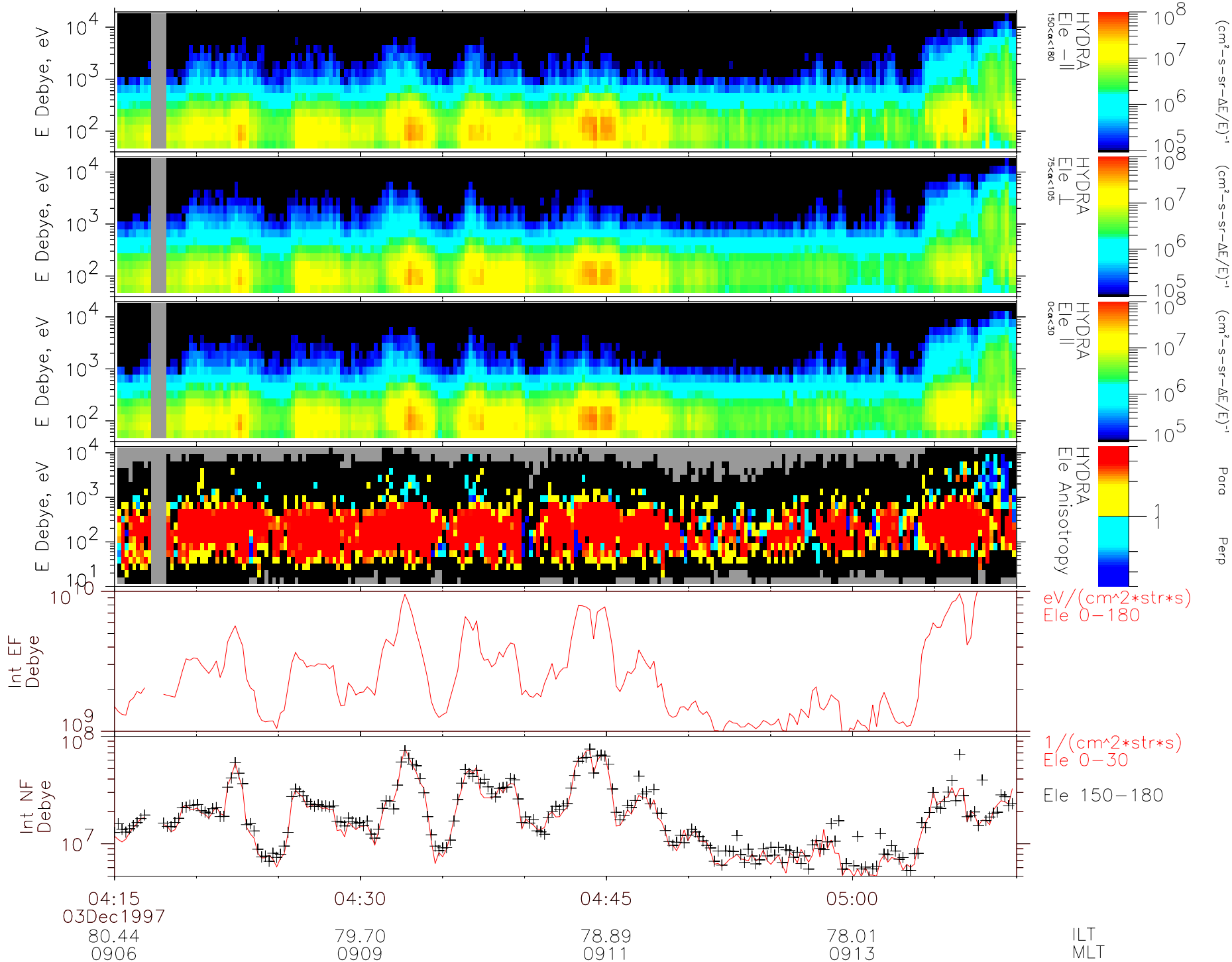

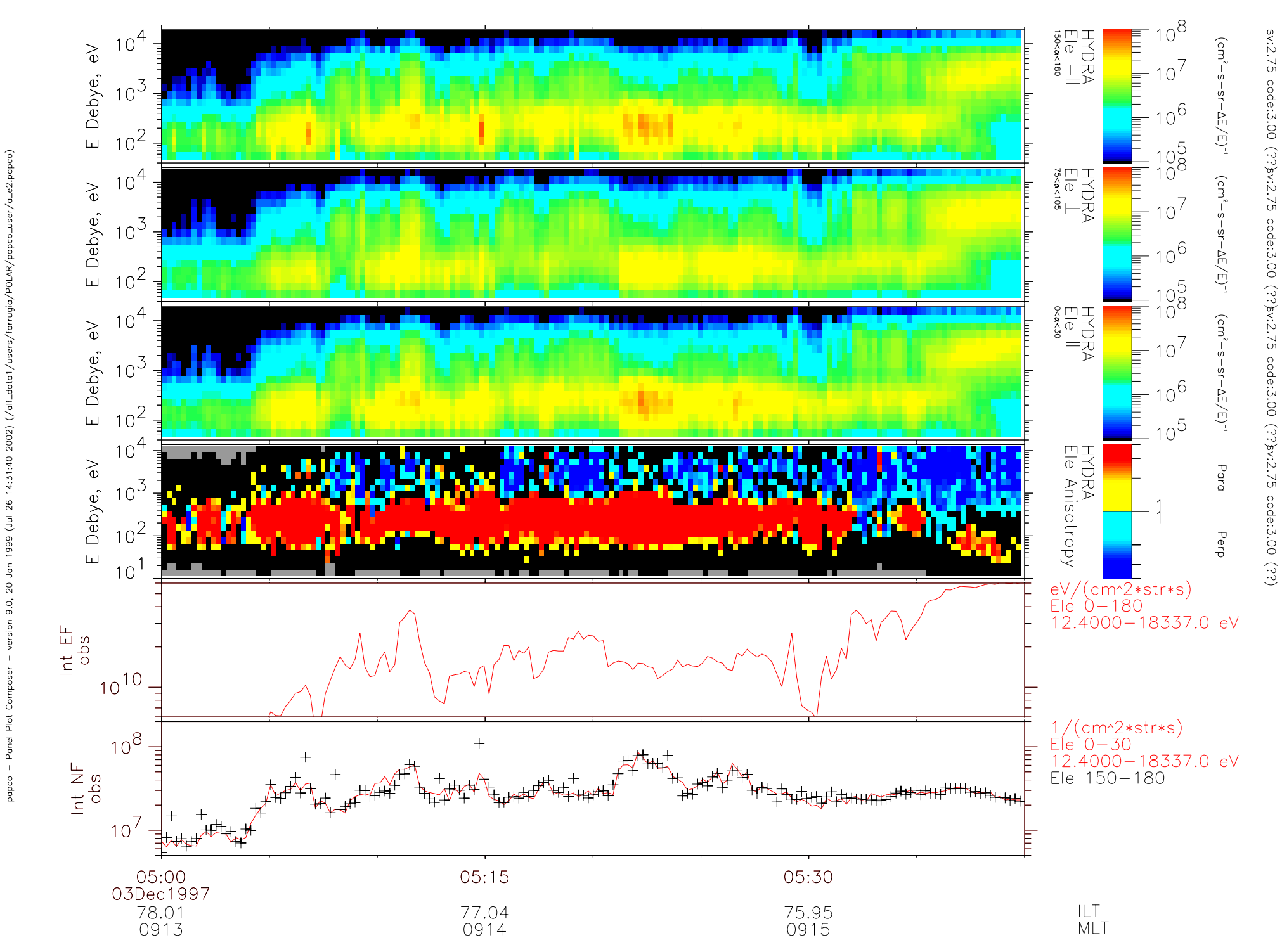
E Debye, eV
HYDRA
Ele −||
150<α<180
HYDRA
Ele ⊥
75<α<105
HYDRA
Ele ||
0<α<30
HYDRA
Ele Anisotropy
(cm²-s-sr-ΔE/E)⁻¹
Para
Perp
Int EF
obs
eV/(cm^2*str*s)
Ele 0−180
12.4000−18337.0 eV
Int NF
obs
1/(cm^2*str*s)
Ele 0−30
12.4000−18337.0 eV
Ele 150−180
05:00
03Dec1997
78.01
0913
05:15
77.04
0914
05:30
75.95
0915
ILT
MLT
papco - Panel Plot Composer - version 9.0, 20 Jan 1999 (Jul 26 14:31:40 2002) (/alf_data1/users/tarrugia/POLAR/papco_user/a_e2.papco)
sv:2.75 code:3.00 (??)

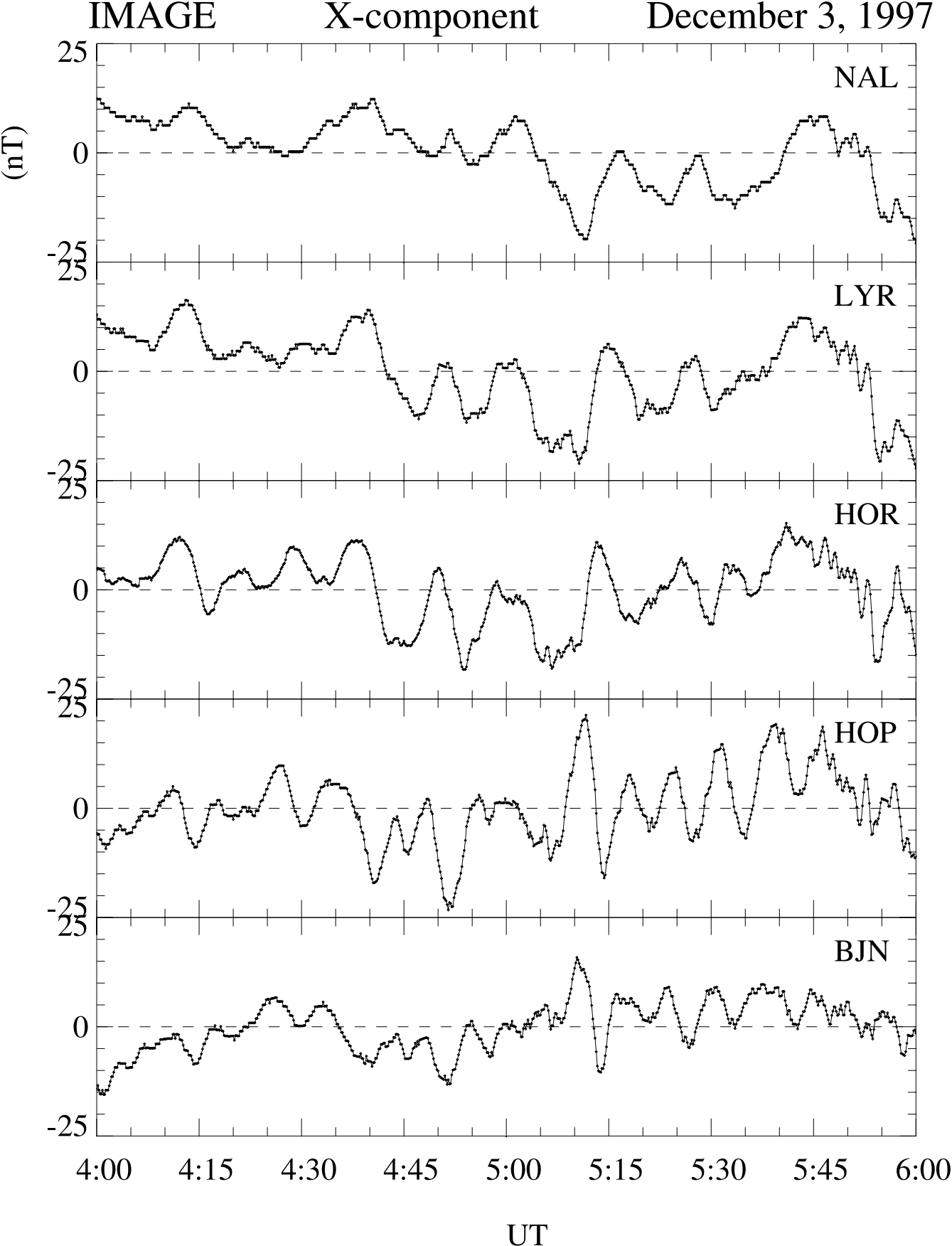
IMAGE X-component December 3, 1997
(nT)
25
0
-25
NAL
LYR
HOR
HOP
BJN
4:00
4:15
4:30
4:45
5:00
5:15
5:30
5:45
6:00
UT

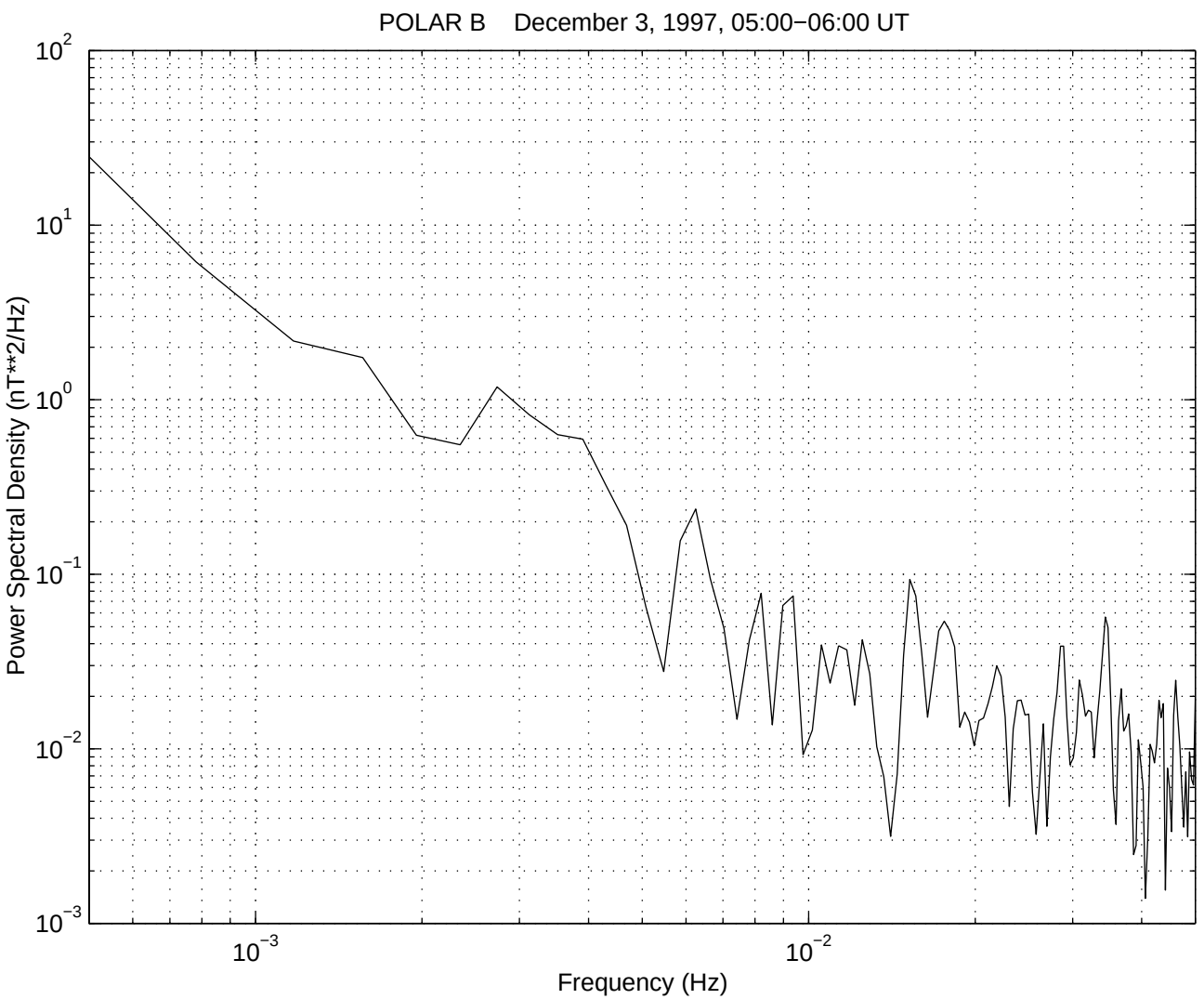
POLAR B December 3, 1997, 05:00−06:00 UT
Power Spectral Density (nT**2/Hz)
Frequency (Hz)
10^2
10^1
10^0
10^−1
10^−2
10^−3
10^−3
10^−2

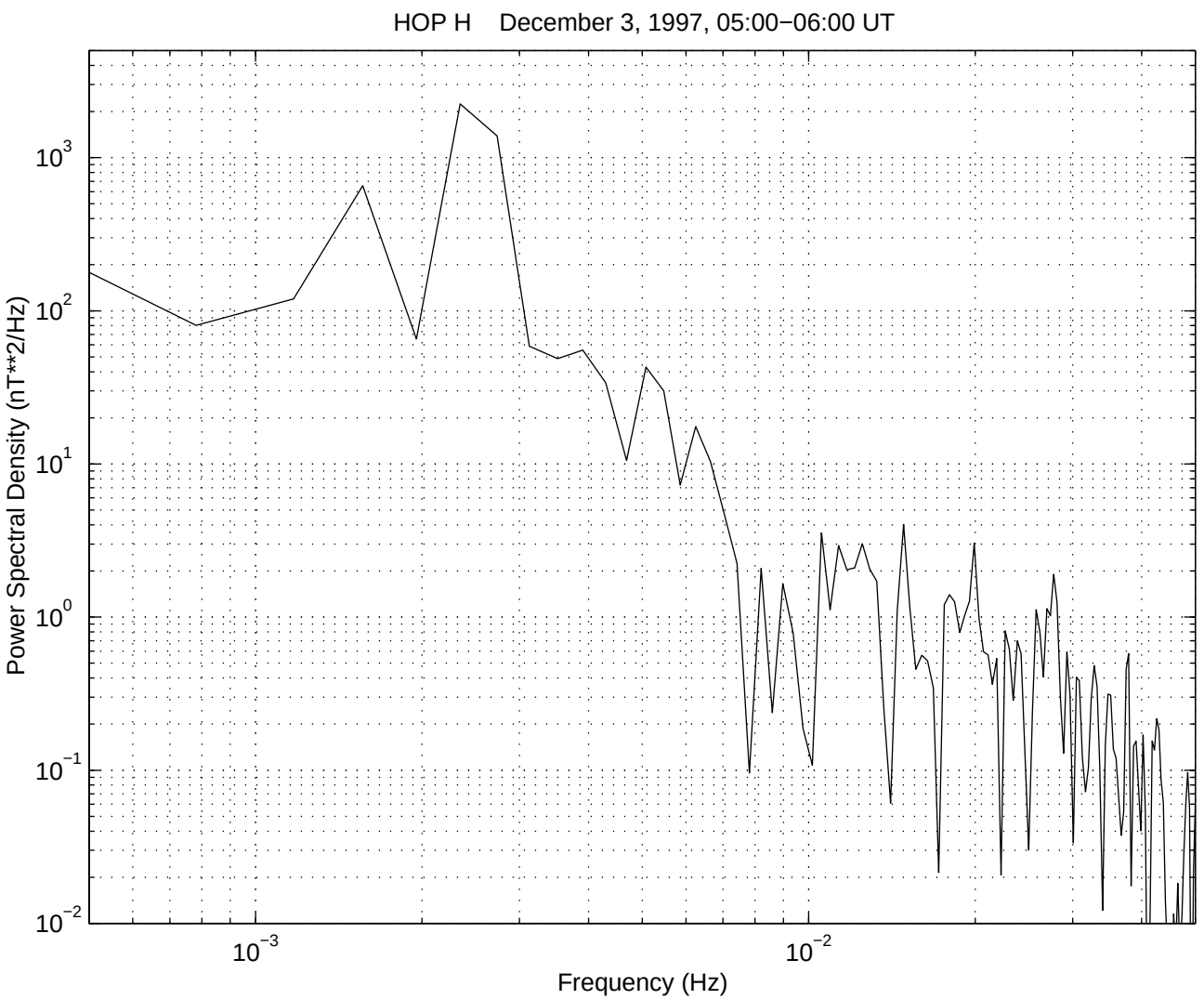
HOP H December 3, 1997, 05:00−06:00 UT
Power Spectral Density (nT**2/Hz)
Frequency (Hz)
10^{3}
10^{2}
10^{1}
10^{0}
10^{-1}
10^{-2}
10^{-3}
10^{-2}

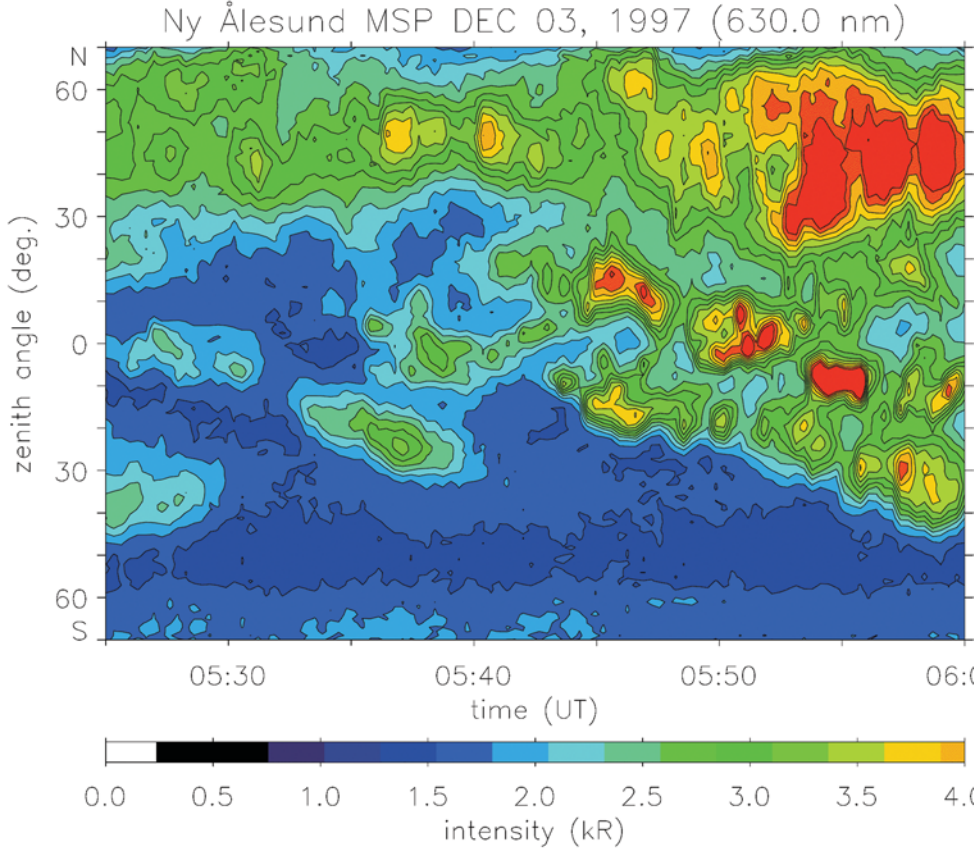
Ny Ålesund MSP DEC 03, 1997 (630.0 nm)
N
60
30
0
30
60
S
zenith angle (deg.)
05:30
05:40
05:50
06:
time (UT)
0.0
0.5
1.0
1.5
2.0
2.5
3.0
3.5
4.
intensity (kR)

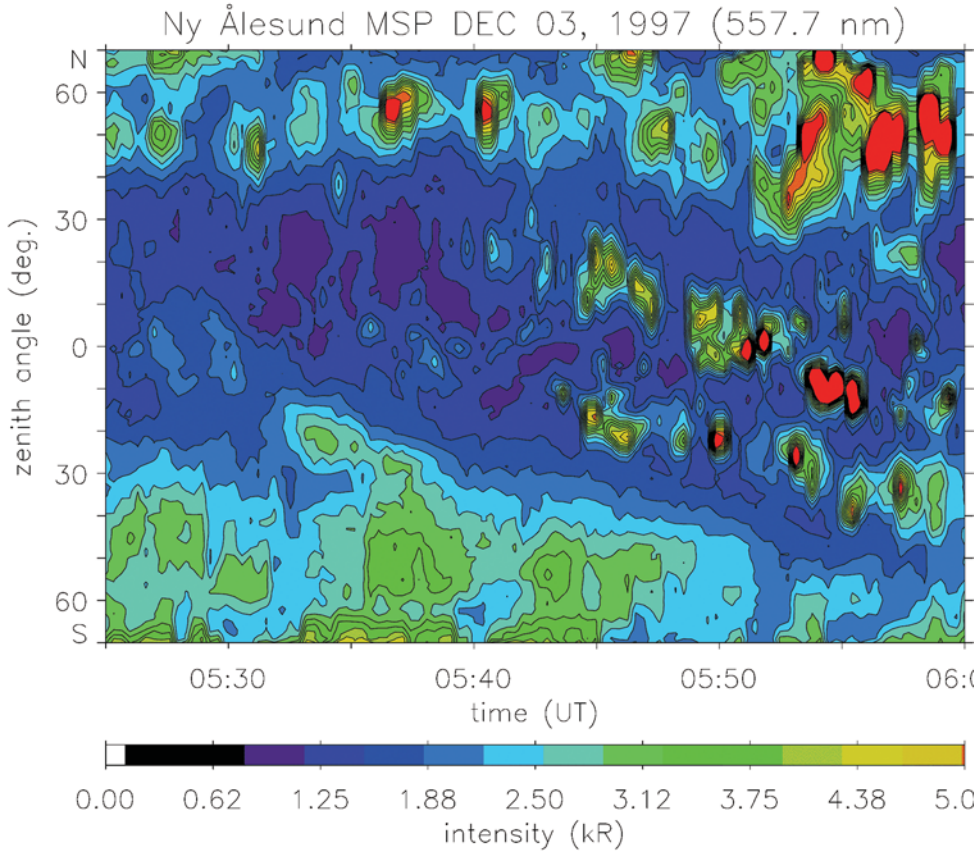
Ny Ålesund MSP DEC 03, 1997 (557.7 nm)
N
60
30
0
30
60
S
zenith angle (deg.)
05:30
05:40
05:50
06:
time (UT)
0.00
0.62
1.25
1.88
2.50
3.12
3.75
4.38
5.0
intensity (kR)

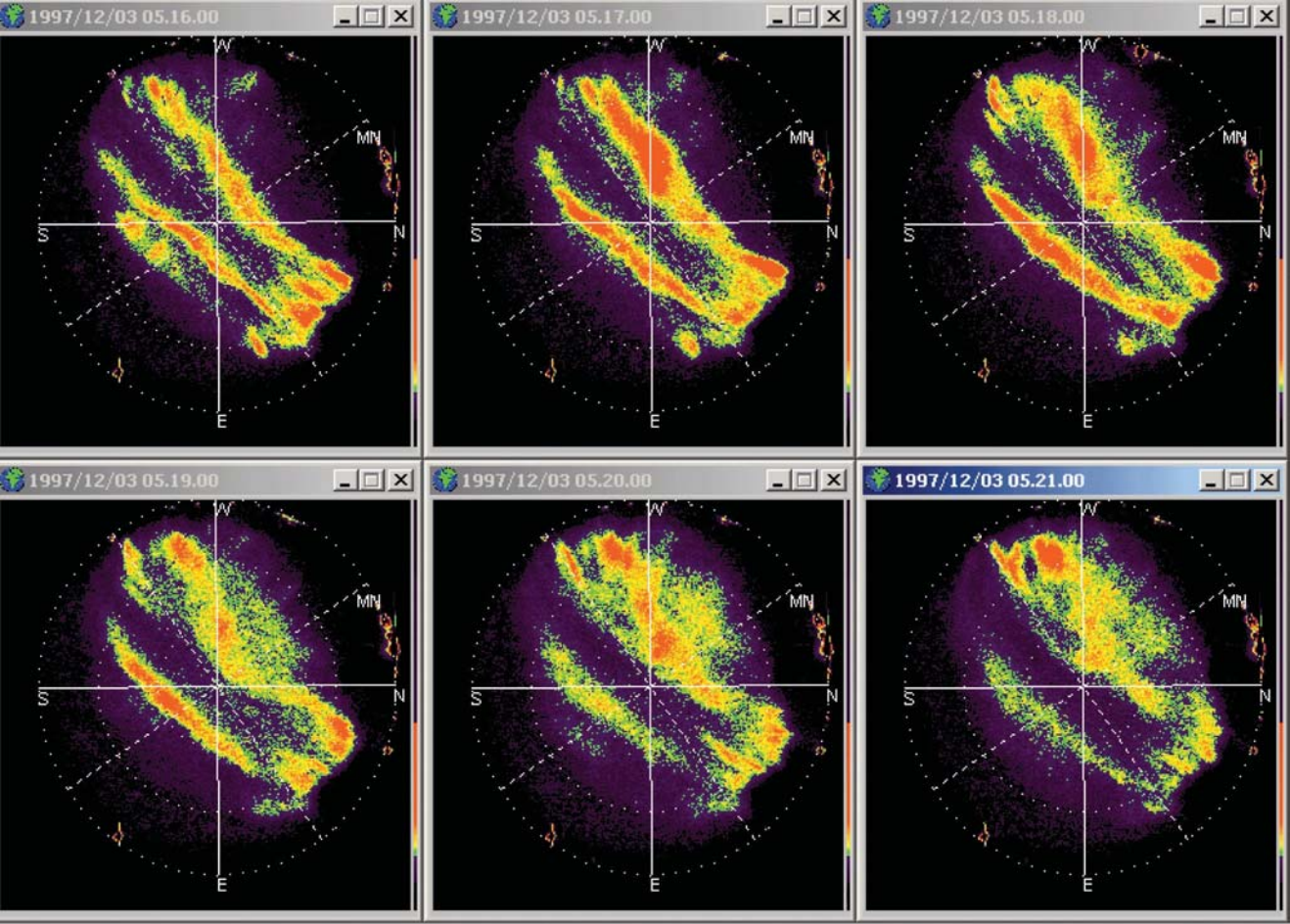
1997/12/03 05.16.00
1997/12/03 05.17.00
1997/12/03 05.18.00
1997/12/03 05.19.00
1997/12/03 05.20.00
1997/12/03 05.21.00
W
MN
S
N
E

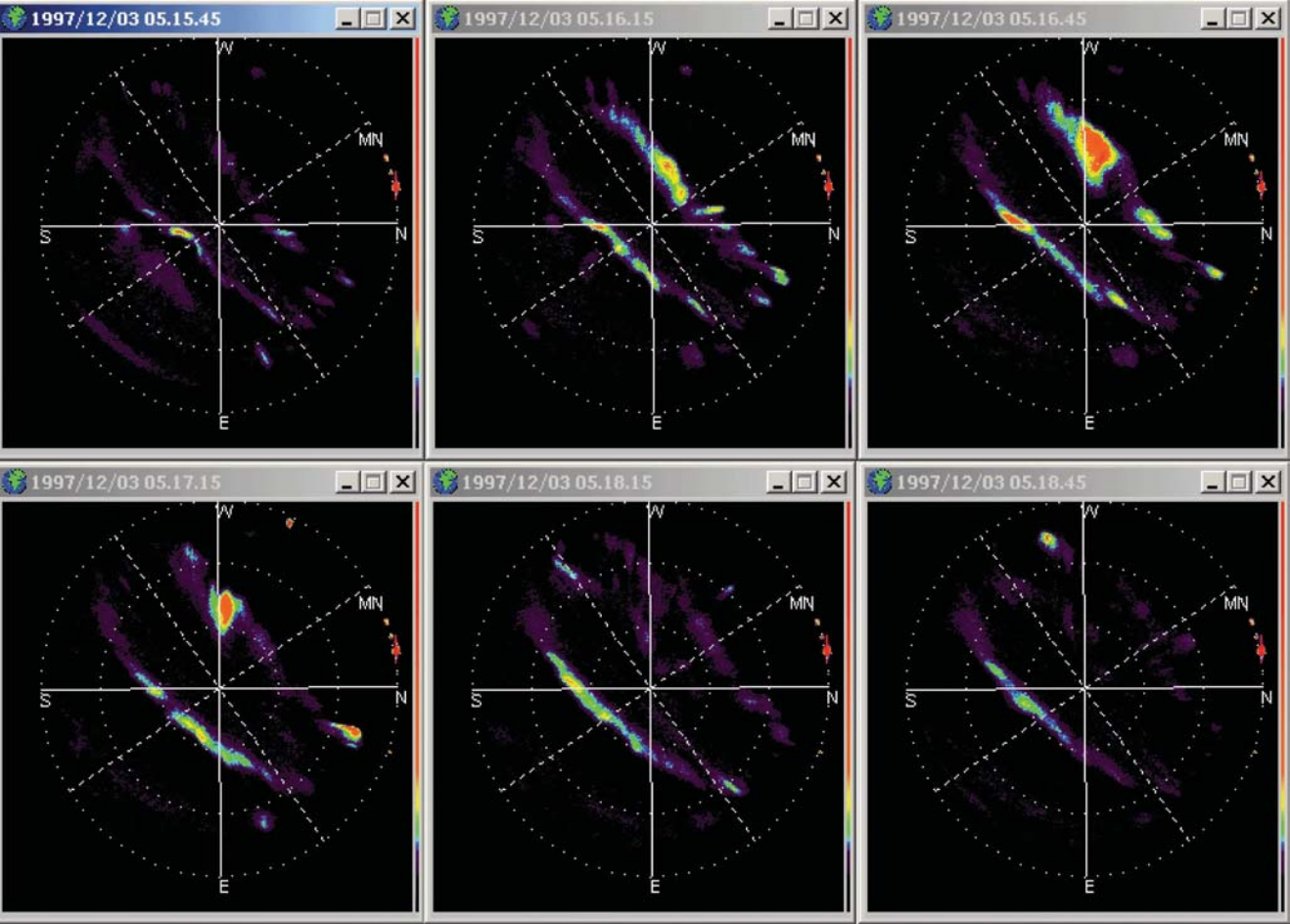
1997/12/03 05.15.45
1997/12/03 05.16.15
1997/12/03 05.16.45
1997/12/03 05.17.15
1997/12/03 05.18.15
1997/12/03 05.18.45
W
MN
S
N
E

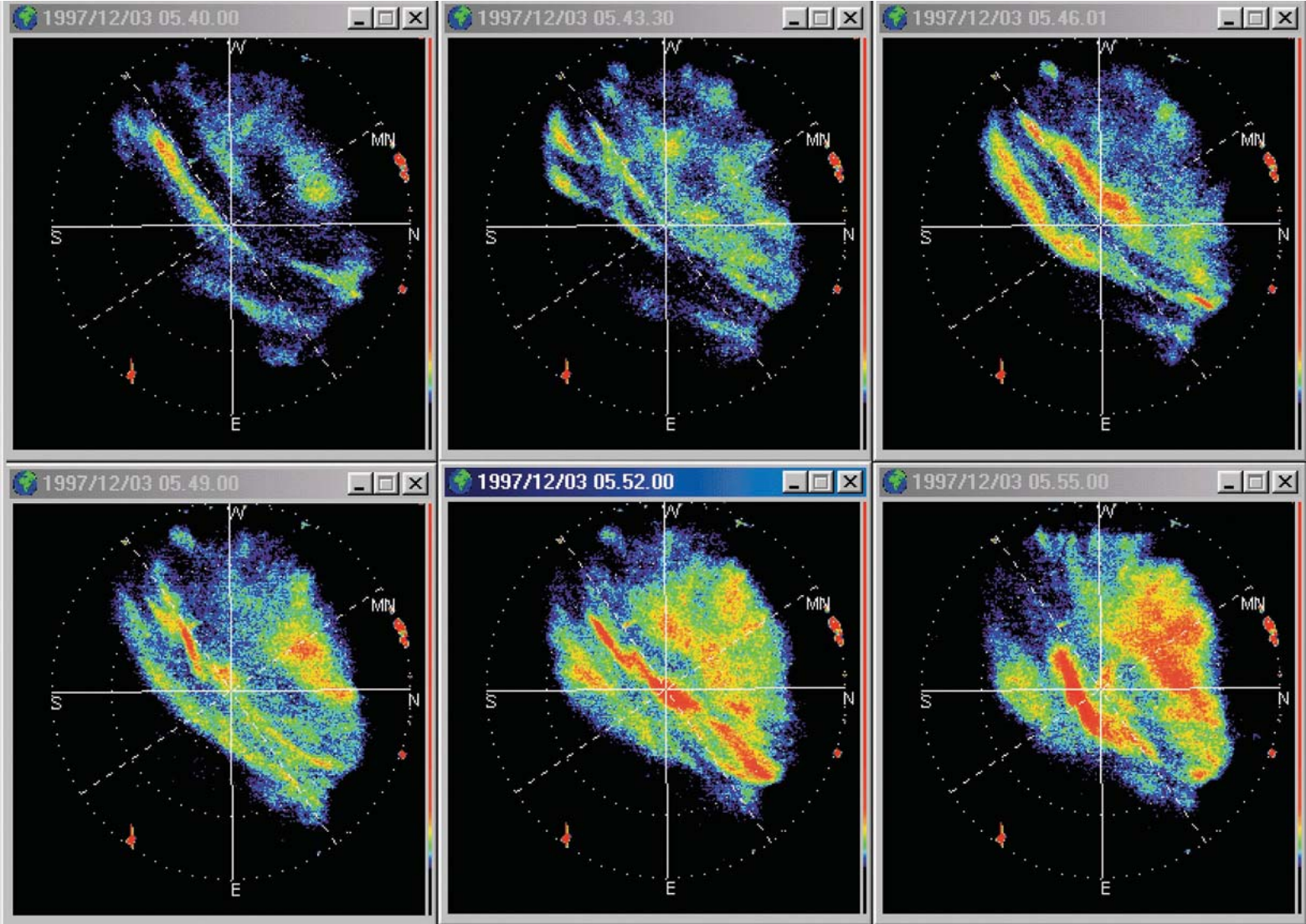
1997/12/03 05.40.00
1997/12/03 05.43.30
1997/12/03 05.46.01
1997/12/03 05.49.00
1997/12/03 05.52.00
1997/12/03 05.55.00
W
MN
S
N
E

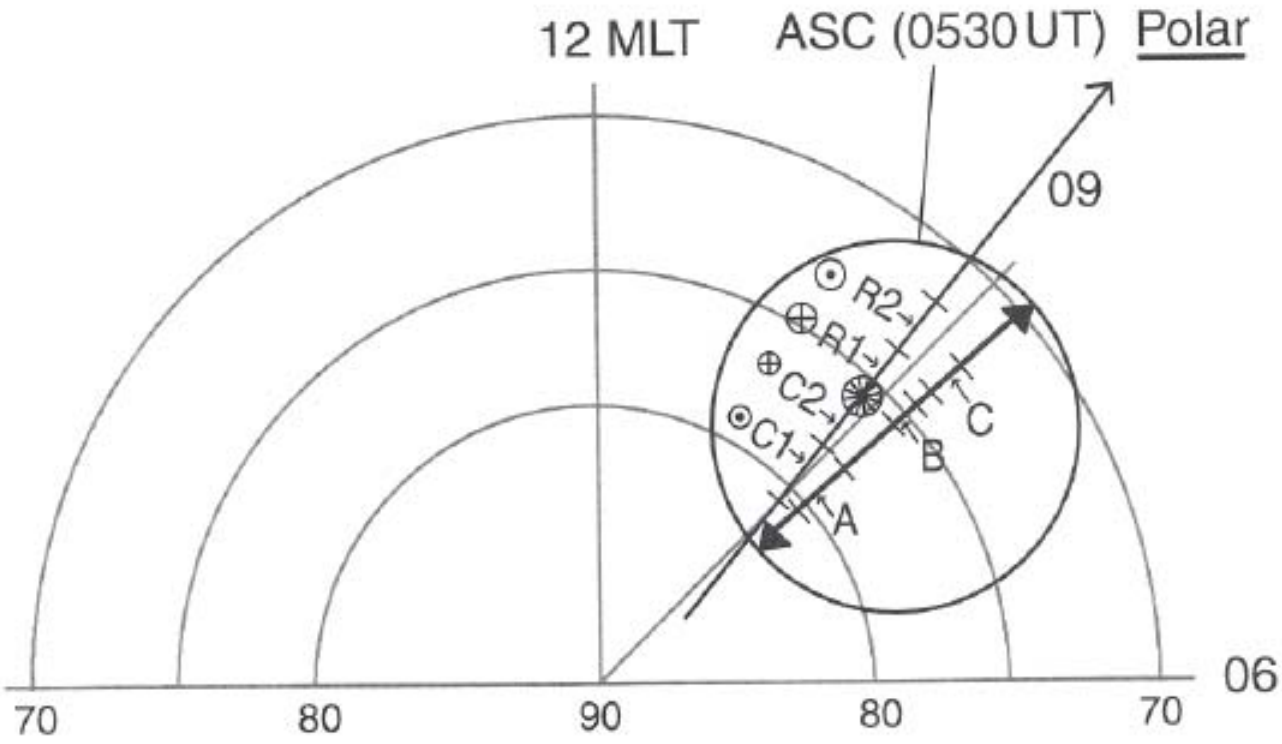

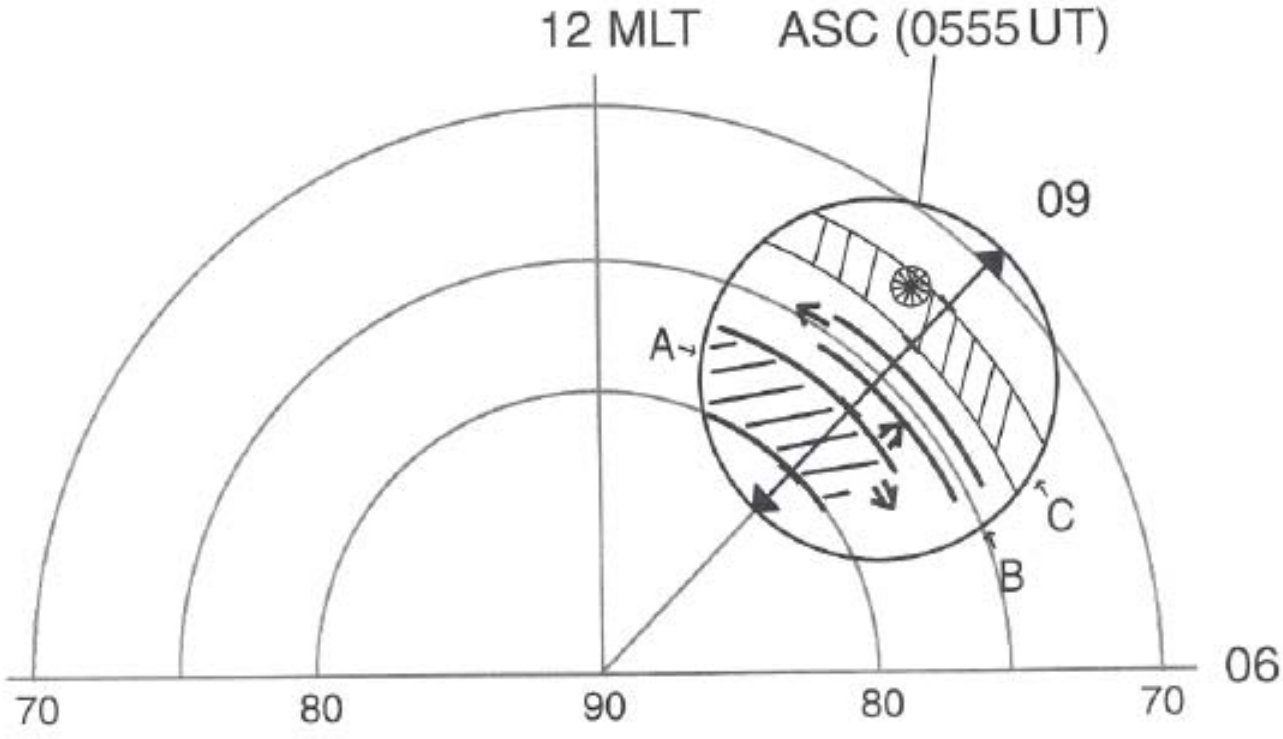

A; cusp-type aurora
B; BPS-type aurora
C; CPS-type aurora
Polar footprint

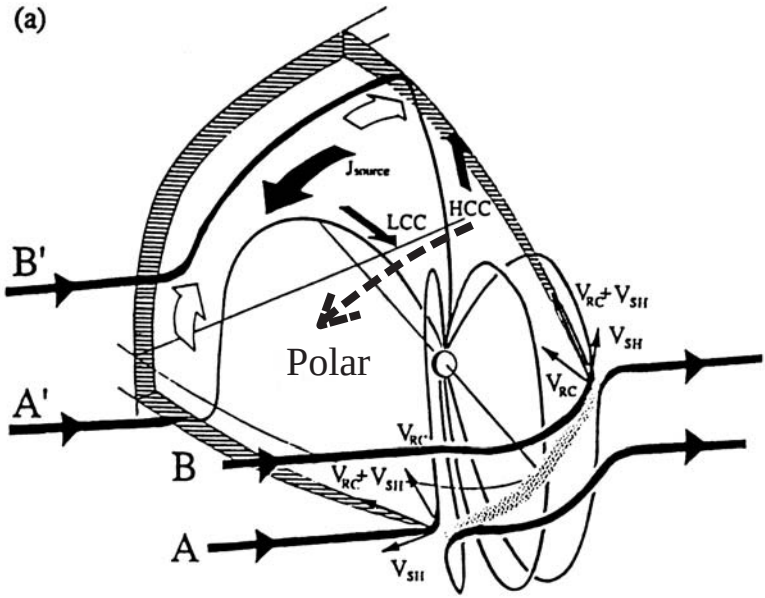
(a)
B'
A'
B
A
Polar
LCC
HCC
J_{source}
$V_{RC}+V_{SH}$
V_{SH}
V_{RC}
$V_{RC}+V_{SH}$
V_{SH}

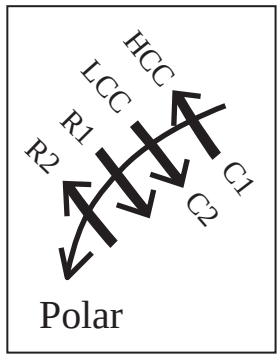
HCC
LCC
R1
R2
C1
C2
Polar

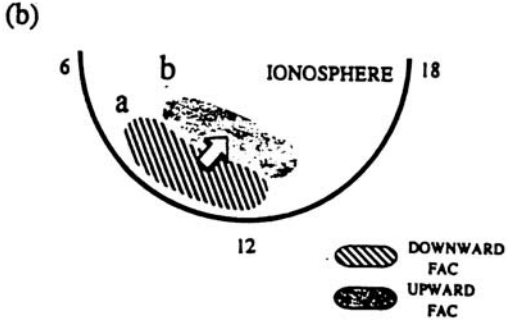
(b)
6
b
IONOSPHERE
18
a
12
DOWNWARD FAC
UPWARD FAC

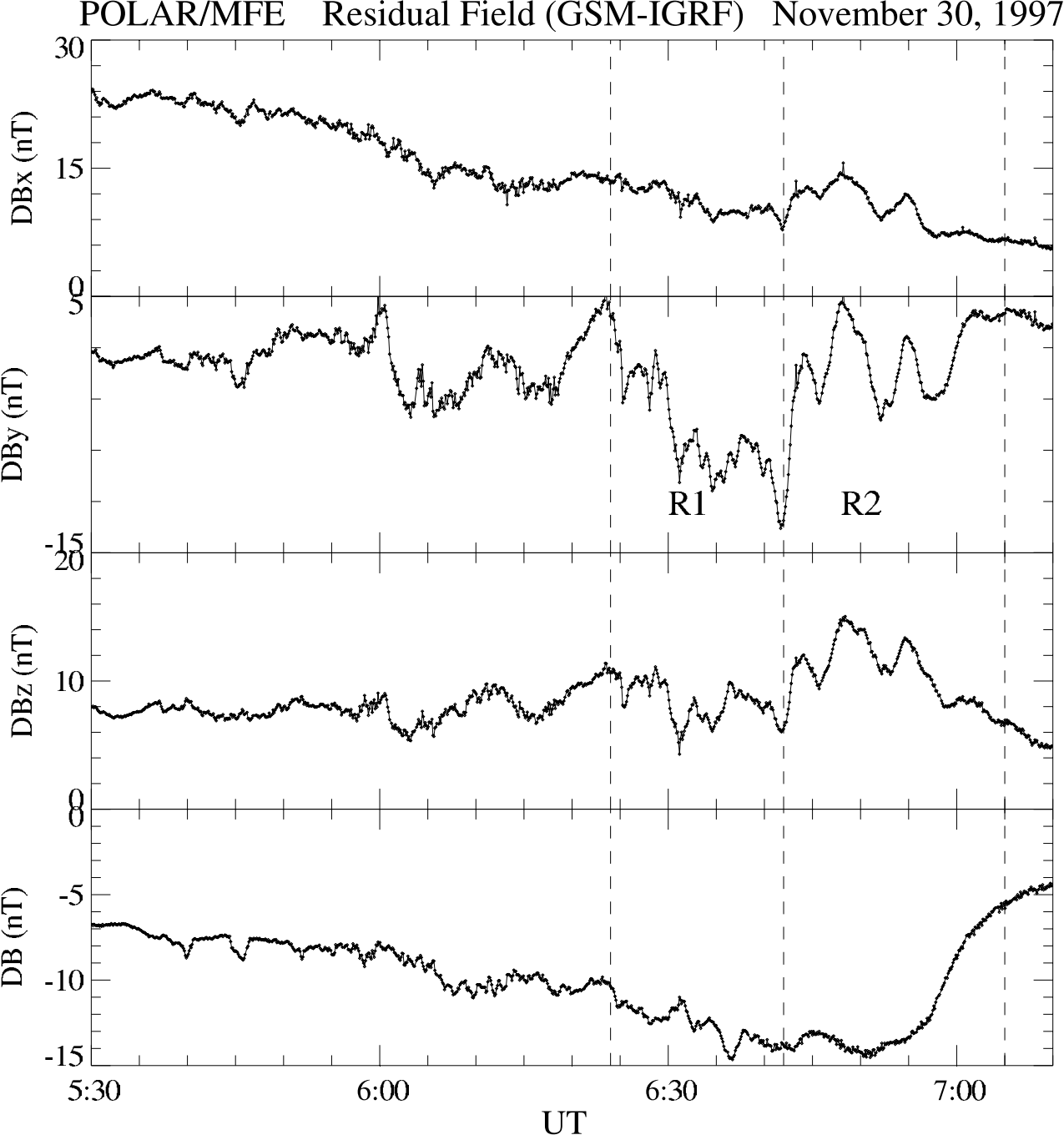
POLAR/MFE Residual Field (GSM-IGRF) November 30, 1997
DBx (nT)
30
15
0
DBy (nT)
5
-15
R1
R2
DBz (nT)
20
10
0
DB (nT)
0
-5
-10
-15
5:30
6:00
6:30
7:00
UT